Self-similar converging magnetohydrodynamic shocks in a quasi-spherical isothermal gas with self-gravity

Bo-Yuan Liu[1]⋆, Yu-Qing Lou[2]

[1]*Department of Physics, Tsinghua University, Beijing, China (PRC)*
[2]*Please fill your information here*

ABSTRACT

We investigated self-similar isothermal magneto-hydrodynamic (MHD) solutions for outgoing or converging envelopes connected by converging isothermal MHD shocks with different core states under quasi-spherical symmetry through a time-reversal operation to the solution space, and discussed possible astrophysical applications of these (self-similar) converging isothermal MHD shock solutions (Shocks). With the introduction of a random traverse magnetic field following the ideal MHD approximation, we developed the MHD version of the self-similar isothermal hydrodynamic (HD) converging shock solutions found by Lou & Shi (2014). Detailed analysis on the time-reversal operation and the new solution space is conducted, based on which we constructed three classes of isothermal MHD converging shock solutions according to the upstream properties near the core, i.e. Class I to III solutions are characterised by MHD Larson-Penston (LP) type, converging MHD void and MHD free-fall collapse asymptotic solution (Yu et al. 2006), respectively. We could also construct twin converging isothermal MHD shock solutions and isothermal MHD converging-shock-rebound-void-expansion-shock (CSRVES) solutions. Despite the versatile behaviours (e.g. winds, outflows, explosions, fall-backs, accretions, collapses, rebounds) of the quasi-spherical system, common properties of our converging isotheraml MHD shock solutions are summarised, which enable us to put forward an overall guideline to construction of expected solutions and identify the general effect of converging isothermal MHD shocks as reversing or enhancing the speed of the outer outgoing or converging envelope and compression of the fluid. As examples, we delineated processes involving such converging isothermal MHD shocks for star formation in magnetised molecular clouds, pre-explosion states and explosions of core-collapse supernovae. With the clearness of solution spaces and the consideration of magnetic fields, our model serves as an useful theoretical tool for understanding the roles played by converging shocks as well as magnetic fields in broad contexts of astrophysics.

Key words: MHD – shock waves – stars: formation – supernovae: general – ISM: clouds

1 INTRODUCTION

Converging shocks with quasi-spherical symmetry can play important roles in many astrophysical processes, e.g. the 'double-detonation' Type Ia supernovae of sub-Chandrasekhar mass white dwarfs (Fink et al. 2007, 2010) and the star formation by collapse of shock-compressed density fluctuations under self-gravity (Klessen 2001). Simulations for progenitor evolutions in the former case have been performed regarding different detonation set-ups of the He-

shell (Fink et al. 2007), as well as different initial core mass and shell mass (Fink et al. 2010). Cylindrical and spherical shocks which may ignite a detonation wave in the deflagration to detonation transition (DDT) are also investigated both analytically and numerically by Kushnir et al. (2012), whose results can be applied to supernovae explosion by setting the criterion of denotation in terms of the shock speed at certain radius from the perspective of ignition mechanism.

In the literature of hydrodynamics, the cylindrically or spherically symmetric converging shock problem in an ideal polytropic gas (inviscid, non-radiating, non-heat-conducting) without self-gravity is referred to as the 'Guder-

⋆ E-mail: liu-by13@mails.tsinghua.edu.cn

ley problem'. Self-similarity method has been applied to the problem as reviewed by Meyer-ter Vehn & Schalk (1982), whose work considers isentropic and non-isentropic self-similar waves, imploding and exploding in the framework of Guderley (1942) with several similarity parameters and critical points. Lazarus (1981) explored the parameter space of such problems regrading the self-similar solutions of converging shocks (non-isentropic) and collapsing cavities (isentropic) with arbitrary adiabatic exponent $\gamma > 1$ in the equation of state $p = K\rho^\gamma$, where p is the pressure, ρ is the mass density, and K is a constant when the entropy is conserved. Self-similar imploding relativistic waves have been studied as the relativistic generalisation of the Newtonian Guderley problem by Hidalgo & Mendoza (2005). Expanding shocks delineated by self-similar solutions are also intensively investigated. For instance, Pan & Sari (2006) studied the relativistic shocks emerging from stars with polytropic envelopes and Oren & Sari (2009) further introduced density perturbations to the former solutions for a strong explosion. Their solutions describe the situation of explosion events (e.g. gamma-ray bursts and supernovae) relevant in very optically thick media such as neutron stars. Generally speaking, the self-similar solutions mentioned above can be divided into two types by the properties of the density profile (Oren & Sari 2009). Type I solution follows the global conservation laws of hydrodynamics and has finite energy, while Type II solution with a steep density profile is characterised by properties near a singular point known as the 'sonic point' which is caused by the rapid acceleration of the shock (Pan & Sari 2006). For these models where the self-gravity is absent, it is the spatial symmetry, the equation state and the restriction on the evolution that determine the behaviour of self-similar solutions. It is also shown that self-similarity method is powerful when states far away from the initial and boundary conditions of the system are considered.

Self-similar solutions for a spherically symmetric isothermal hydrodynamic (HD) system with self-gravity are also valuable. For example, the well-known outflow solution with $\rho \propto r^{-2}$ and $v = 3.3c$, where ρ is the mass density, r is the radius, v is the velocity of the fluid, and c is the speed of sound, as $t \to 0$ or $r \to \infty$ by Larson (1969) and Penston (1969) (the LP-type solution) can be applied to the outside-in collapse of star formation after a time-reversal operation. Besides, a free-fall inner envelope with $\rho \propto r^{-3/2}$ as $t \to \infty$ or $r \to 0$ can be connected to the static or nearly static outer envelope similar to that of the LP solution (Shu 1977), which is known as the expansion-wave collapse solution (EWCS) describing a self-similar inside-out collapse. Another progress regarding such a system is made by Hunter (1977) through his invention of a matching method in density-velocity (as dimensionless parameters after the self-similar transformation of variables) phase diagrams and exploration of new self-similar solutions for the inner envelope other than free-fall solutions. Moreover, Whitworth & Summers (1985) enlarged the discrete solutions found by former authors with the concept of weak discontinuities across the sonic critical line (SCL) which divides the solution space into the subsonic region and the supersonic region. In the same work, two types of sonic points (saddle points and nodal points) on the SCL are also defined related to the stability of solutions crossing it. The

studies mentioned above constructed self-similar solutions by connecting different asymptotic solutions with numerical integrations of the same set of non-linear ordinary differential equations (ODEs) derived from the original non-linear HD partial differential equations (PDEs) through the self-similar transformation. As a standard research of this type, Lou & Shen (2004) further explored the 'semi-complete solution space' and constructed envelope expansion core collapse (EECC) solutions which feature concurrent interior core collapse and exterior envelope expansion pertinent to proto-planetary nebula and certain evolution phase of galaxy clusters.

More importantly, it is possible to add shocks into isothermal self-similar solutions with self-gravity and spherical symmetry by certain shock conditions. The shock can be used to connect different asymptotic solutions which cannot be connected merely by numerical integrations and alter the accretion rate as well as other parameters in the centre (Tsai & Hsu 1995). Such self-similar isothermal hydrodynamic shock solutions[1] were intensively studied in the context of astrophysics, e.g. the photo-ionization stellar wind in planetary nebulas (Chevalier 1997), the self-similar champagne flows in H_{II} regions (Shu et al. 2002), the dynamical evolution phase of younger stellar objects (Shen & Lou 2004), the dynamical connection between the asymptotic giant branch to proto-planetary nebula phase (Bian & Lou 2005), and the voids in surrounding envelopes for hot bubbles in the interstellar medium as well as supernovae remnants (Lou & Zhai 2009), in that such shock solutions can accommodate dynamical processes of outflows, inflows, subsonic oscillations, free-fall core collapse and voids (Bian & Lou 2005; Lou & Zhai 2009). The temperatures in the regions behind and ahead the shock front can be the same or different from each other, and the shock conditions are derived from the conservation of mass and momentum with proper entropy variations.

Additionally, in a more complicated case with a random magnetic field, isothermal shock solutions for magneto-hydrodynamic (MHD) gas were worked out by Yu et al. (2006). Moreover, the state of the gas is not limited to be isothermal. In general, self-similar shock solutions were also constructed in an ordinary conventional or general polytropic gas (Lou & Gao 2006; Lou & Wang 2006, 2012; Hu & Lou 2008; Lou & Cao 2008) or in the MHD version of that (Wang & Lou 2008; Lou & Hu 2010). Despite the abundance of aforementioned literatures, only expansion shocks are investigated in these models, while self-similar converging shocks are less thoroughly studied.

As a key reference of the present work, Lou & Shi (2014) derived several self-similar converging HD shock solutions for an isothermal spherically symmetric ordinary gas and analysed their applications on star formation, supernovae and collapsing voids. Since magnetic fields play important roles in a variety of astrophysical environments (e.g. dramatically increasing mass-to-flux ratio related to static field supporting, ambipolar diffusion, and Alfvénic motion dur-

---

[1] Sometimes, for conciseness, we use the word 'Shock' representing the phrase 'shock solution' to indicate the whole self-similar solution involving shock(s), while the word 'shock' means simply the shock itself.

ing star formation in magnetised molecular clouds (McKee & Ostriker 2007; Crutcher 1999)), it would be more realistic to take them into account. In the light of this, the aim of the present study is to construct self-similar converging isothermal MHD shock solutions by connecting different self-similar solutions of an isothermal magneto-fluid under quasi-spherical symmetry as shown in Yu & Lou (2005) with converging isothermal MHD shocks. Some solutions may serve as the MHD counterparts of those in Lou & Shi (2014). In this way, we may better appreciate relevant astrophysical processes in consideration of a random traverse magnetic field under the ideal MHD approximation. Following the propagation direction of the shock , we define the region behind the shock front as the downstream, while that ahead the shock front as the upstream. It will be shown later in Section 3.1 that due to the nature of our self-similar method, the upstream is also the side of the shock front through which the gas enters, i.e. the so-called *front side* in Courant & Friedrichs (1976), while the downstream the *back side*. Unlike the case of Lou & Shi (2014), this definition is independent of the time-reversal operation. Then by the second law of thermodynamics, the effective entropies of these two regions satisfy the inequality: $s_d - s_u \geq 0$, where s_d is the effective entropy at the downstream side and s_u the upstream side. Here the effective entropy is defined from the perspective of thermodynamics as followings: For an ideal gas (whose internal energy per unit mass e depends only on the temperature T) with the equation of state $p = (k_B/\mu) \cdot T\rho = R \cdot T\rho$, where k_B is the Boltzmann constant, and μ is the average mass of one gas molecule, we have the entropy per unit mass $S = c_v(T)\ln\left[p\rho^{-\gamma}/(\gamma - 1)\right] + S_0$, where $c_v(T) = R/(\gamma - 1)$ is the isometric heat capacity per unit mass, and $\gamma = \gamma(T) = 1 + R(dT/de)$ is a dimensionless quantity as a function of T (Courant & Friedrichs 1976). For a polytropic gas in which γ (i.e. the polytropic index) as well as c_v is constant, since it is only the variance of the entropy that is concerned, for conciseness, we define the effective entropy as $s = \ln(p/\rho^\gamma)$. Time-reversal operation $t \to -t$ (see Section 2.2 for details) is performed to construct such converging isothermal MHD shocks under an extended version of the isothermal MHD shock conditions in Yu et al. (2006) which are meant for 'outgoing' isothermal MHD shocks, however, with different correspondences between the downstream or upstream and the inner or outer region of the solution space. Without special annotation, any result in this paper is displayed in the solution space after the time-reversal operation (i.e. the new solution space) .

The basic MHD model formulation for our converging isothermal MHD shock problem including MHD PDEs, the self-similar MHD transformation as well as the ODEs reduced from it, the time-reversal operation and known asymptotic solutions are contained in Section 2. One-temperature and two-temperature isothermal MHD shock conditions are presented in Section 3. Results of self-similar isothermal MHD void solutions, three classes of converging isothermal MHD shock solutions and twin converging isothermal MHD shock solutions calculated by numerical integrations with the standard 4-order Runge-Kutta method are displayed in Section 4, 5 and Appendix E. Discussions on the general empirical guideline that could be given in search of such converging isothermal MHD shock solutions

and some astrophysical applications are included in Section 6.

2 THE BASIC MHD MODEL

2.1 From PDEs to ODEs

The magnetic field in this paper is a tangled traverse magnetic field, whose effect is embodied by the magnetic pressure and tension force terms in the equation of radial component momentum conservation. To reach the quasi-spherical symmetry, some terms of the original MHD momentum equations are ignored (see Appendix C in Yu & Lou (2005) for details), despite that in practice these terms may break the quasi-spherical symmetry[2]. In the spherical polar coordinates (r, θ, ϕ), with the magnetic field delineated by an average $\langle B_{||}^2 \rangle$, where $B_{||} = (B_\theta^2 + B_\phi^2)^{1/2}$ stands for the component parallel to the isothermal MHD shock front (i.e. tangent to the sphere surface), we adopt a specific equation of state for an isothermal ideal gas $p = a^2\rho$, where p is the pressure, ρ is the mass density, and a is the isothermal sound speed, and write down the following MHD PDEs:

$$\frac{\partial \rho}{\partial t} + \frac{1}{r^2}\frac{\partial\left(r^2\rho u\right)}{\partial r} = 0 \; , \tag{1}$$

$$\frac{\partial M}{\partial r} = 4\pi\rho r^2, \qquad \frac{\partial M}{\partial t} + u\frac{\partial M}{\partial r} = 0 \; , \tag{2}$$

$$\frac{\partial u}{\partial t} + u\frac{\partial u}{\partial r} = -\frac{a^2}{\rho}\frac{\partial \rho}{\partial r} - \frac{GM}{r^2} - \frac{1}{8\pi\rho}\frac{\partial}{\partial r}\langle B_{||}^2\rangle - \frac{\langle B_{||}^2\rangle}{4\pi\rho r} \; , \tag{3}$$

where PDEs (1) and (2) represent conservation of mass, PDE (3) stands for MHD radial momentum conservation, $u(r, t)$ is the radial flow speed, $M(r, t)$ is the mass enclosed within radius r at time t, and $G = 6.67\times10^{-8} \; \mathrm{g}^{-1}\cdot\mathrm{cm}^3\cdot\mathrm{s}^{-2}$ is the universal gravitational constant. Unlike the generalized version of our model, i.e. the quasi-spherical MHD model of a general polytropic magneto-fluid (Wang & Lou 2008), here we do not explicitly include the equation of effective entropy conservation

$$\left(\frac{\partial}{\partial t} + u\frac{\partial}{\partial r}\right)\left(\ln\frac{p}{\rho^\gamma}\right) = 0 \; , \tag{4}$$

where γ is the polytropic index. Actually, in our model, only when $\gamma \to 1$, the effective entropy $s = \ln(p/\rho^\gamma) \to 2\ln a$ is conserved, in which case (, for regions other than near the shock front), our model actually describes an adiabatic process which meanwhile has a constant temperature. If we discard the requirement of effective entropy conservation, γ becomes an adjustable parameter which also denotes the ratio of the isobaric heat capacity and the isometric heat capacity (e.g. $\gamma = 4/3$ for the relativistic perfect gas and $\gamma = 5/3$ for the non-relativistic perfect gas), and the isothermal sound speed $a = A/\gamma^{1/2} \neq A$, where A is the adiabatic sound speed.

With the ideal MHD approximation of infinite conductivity (see Appendix A), we can show that (Yu et al. 2006)

$$B_{||}/(\rho r) = \mathrm{const.} \tag{5}$$

---

[2] Our model is based on the randomness of the transverse magnetic field which presupposes that contributions of these terms cancel each other or are negligible on certain scales.

from which we further introduce the dimensionless parameter λ by

$$\lambda \equiv B_{||}^2 / \left(16\pi^2 G \rho^2 r^2 \right) \ . \tag{6}$$

We define the dimensionless independent self-similar variable as $x \equiv r/(at)$ and perform the following self-similar MHD transformation to PDEs (1)-(3):

$$\rho(r,\ t) = \frac{\alpha(x)}{4\pi G t^2}, \qquad M(r,\ t) = \frac{a^3 t}{G} m(x) \ ,$$
$$u(r,\ t) = a v(x), \qquad B_{||}(r,\ t) = \frac{ab(x)}{\sqrt{G} t} \ , \tag{7}$$

where $\alpha(x) \geq 0$, $m(x)$, $v(x)$ and $b(x)$ are the reduced dimensionless variables as functions of x for the mass density, the enclosed mass, the radial flow speed and the transverse magnetic field strength, respectively. From flux conservation integral (6), we have $b(x) = \sqrt{\lambda}\alpha x$. Similarly, the Alfvén wave speed defined as $v_A \equiv B_{||}/\sqrt{4\pi\rho}$ can be expressed with dimensionless variables and the isothermal sound speed: $v_A = \sqrt{\lambda\alpha} \cdot xa$.

It follows that PDEs (2) become

$$m' = x^2 \alpha, \qquad (v - x)m' + m = 0 \ , \tag{8}$$

where the prime stands for the derivative with respect to x. These two nonlinear ODEs can be further combined to give

$$m = (x - v)x^2 \alpha \ , \qquad \left[x^2 \alpha (x - v) \right]' = x^2 \alpha \ , \tag{9}$$

the first one of which indicates that the solutions of v are restricted in the upper-right region with respect to the straight line $x - v = 0$ in the $-v$ versus x plane due to the physical requirement of positive enclosed mass, i.e. $m(x) \geq 0$, when $t > 0$. In Section 4, solutions which hit the $x - v = 0$ line can be regarded as MHD void solutions with a central void in expansion (without the time-reversal operation) or contraction (after the time-reversal operation) surrounded by a dynamic envelope. And the straight line $x - v = 0$ is referred to as the zero mass line (ZML).

PDE (1) can be reduced to

$$v' + (v - x)\alpha'/\alpha = 2(x - v)/x \ , \tag{10}$$

while by ODE (9) and the self-similar MHD transformation, PDE (3) (multiplied by a factor of t/a on both sides) takes the form

$$(v - x)v' = -\alpha' \left(1/\alpha + \lambda x^2 \right) - 2\lambda\alpha x - \alpha(x - v) \ . \tag{11}$$

Through simple algebra, with ODEs (10) and (11), we derive the final two coupled non-linear MHD ODEs (which are applied to numerical integrations by the Runge-Kutta method in Section 4, 5 and Appendix E) as followings:

$$\left[(x - v)^2 - \left(1 + \lambda\alpha x^2 \right) \right] v' = (x - v) \left[\alpha(x - v) - \frac{2}{x} \right] \ , \tag{12}$$

$$\left[(x - v)^2 - \left(1 + \lambda\alpha x^2 \right) \right] \alpha' = (x - v) \left[\alpha^2 - \frac{2\alpha}{x}(x - v) \right]$$
$$+ 2\lambda\alpha^2 x \ . \tag{13}$$

The above two coupled non-linear ODEs can be written in the compact forms of $F_x(x,\ v,\ \alpha)v' = F_v(x,\ v,\ \alpha)$, $F_x(x,\ v,\ \alpha)\alpha' = F_\alpha(x,\ v,\ \alpha)$ with three functionals F_x, F_v, and F_α naturally defined. Apparently, these

ODEs have singularity in the case that $F_x = 0$[3], where we must require that $F_v = F_\alpha = 0$, simultaneously in order to have finite smooth solutions in a consistent manner across the magnetosonic critical line/curve (MSCL/MSCC) specified by

$$x - v = 2/(\alpha x) \ , \qquad x - v + 2\lambda x = (x - v)^3 \ , \tag{14}$$

on which detailed analysis can be found in Yu & Lou (2005).

2.2 Time-reversal operation

As for the time-reversal operation $t \to -t$, it is shown from the definition of x that $x \to -x$. Besides, by additional variable transformation $v \to -v$ (with α and b unchanged), from ODEs (9), it turns out that $m \to -m$, and the forms of ODEs (8)-(14) are reserved, which offers great convenience to our model analysis. Now we regard x, v, α, m and b as variables after the time-reversal operation (the new solution space), and note the original self-similar dimensionless variables as $\widetilde{x}$, $\widetilde{v}$, $\widetilde{\alpha}$, $\widetilde{m}$ and $\widetilde{b}$ (the old solution space). Following the relations between the two solution spaces, i.e. $\widetilde{x} = -x$, $\widetilde{v} = -v$, $\widetilde{\alpha} = \alpha$, $\widetilde{m} = -m$, and $\widetilde{b} = b$[4], we note down the complete self-similar transformation that indicates the relations between physical quantities and self-similar variables in both the new and the old solution space:

$$\rho = \frac{\widetilde{\alpha}}{4\pi G t^2} = \frac{\alpha}{4\pi G t^2} \ , \quad M = \frac{a^3 t}{G}\widetilde{m} = -\frac{a^3 t}{G}m \ ,$$
$$u = a\widetilde{v} = -av \ , \quad B_{||} = \frac{a\widetilde{b}}{\sqrt{G} t} = \frac{ab}{\sqrt{G} t} \ , \quad r = at\widetilde{x} = -atx \ , \tag{15}$$

by which we obtain physical interpretations of our self-similar MHD (shock) solutions in the new solution space when $t < 0$ (i.e. $x > 0$), while the old solution space when $t > 0$ (i.e. $\widetilde{x} > 0$).

Actually, some types of solutions are named by their physical interpretations in the old solution space, say the EWCS and the free-fall collapse solution. The problem is that the interpretations are different or even unrealistic in the new solution space. In this paper, we reserve the name 'EWCS' and 'free-fall collapse' from the perspective of features of the self-similar solution itself (which remain unchanged in the new solution space compared with those in the old solution space), instead of their physical meanings. In fact, after the time-reversal operation, the so-called EWCS means converging-wave-core-expansion and the nominal free-fall collapse solution indicates free-expansion.

In fact, our definitions of the upstream and the downstream of the isothermal MHD shock are purely from the perspective of the second law of thermodynamics, i.e. $s_d > s_u$, and, therefore, independent of the time-reversal operation. Such definitions leave the physical meanings unchanged, however, imply that correspondences between the upstream side and the downstream side with different parts

---

[3] It is equivalent to the equation $a^2(v - x)^2 = a^2 + v_A^2$ which is related to the fast magneto-sonic condition.
[4] The expression of the Alfvén wave speed $v_A = \sqrt{\lambda\alpha}x \cdot a$ remains unchanged after the reversal operation. So does the requirement that $m \geq 0$, in that when $t < 0$, for $M(r,\ t) \geq 0$, we must have $-m = \widetilde{m} \leq 0$.

of the solution space will reverse after the time-reversal operation (,in that we shift from the old solution space to the new solution space). That is to say, for converging isothermal MHD shock solutions in the new solution space, $-\infty < t < 0$, $0 < x < +\infty$, and the part that comes from near the origin $x = -\tilde{x} = -r/(at) \to 0_+$ as $r \to 0$ or $t \to -\infty$ corresponds to the upstream side, while the part that comes from the infinity $x \to +\infty$ as $r \to +\infty$ or $t \to 0_-$ corresponds to the downstream side, since converging shocks propagate towards the centre and the increase of x in such a case means that we go from the past to the future (with a larger t and smaller $|t|$) or from the inner part to the outer part (with a larger r).

2.3 Known asymptotic solutions

Only given certain asymptotic isothermal MHD solution near certain value of x (e.g. $x \to 0_+$, $x \to +\infty$, and near the MSCL) to provide the initial condition, could numerical integrations be conducted. This section lists the asymptotic solutions of Yu & Lou (2005) and Yu et al. (2006) without presenting relevant derivations in detail. Generally speaking, there are three methods of attaining asymptotic solutions: Taylor or Laurent expansion, retaining proper terms in the MHD ODEs (balance of dominant terms), and the L'Hospital's rule.

In the limit of $x \to +\infty$, assuming that $v \to V$, while $\alpha \to A/x^2$, using Laurent expansion, from the MHD ODEs (12) and (13), we have

$$v(x) = V + \frac{2-A}{x} + \frac{V}{x^2}$$
$$+ \frac{(A/6-1)(A-2) + 2V^2/3 + A(2-A)\lambda/3}{x^3} + \dots , \quad (16)$$

$$\alpha(x) = \frac{A}{x^2} + \frac{A(2-A)}{2x^4} + \frac{A(4-A)V}{3x^5}$$
$$+ \frac{A(A-3)(A/2-1) - (A-6)AV^2/4 + A^2(2-A)\lambda/4}{x^6} + \dots , \quad (17)$$

$$b^2(x) = \frac{A^2\lambda}{x^2} + \frac{A^2(2-A)\lambda}{x^4} + \frac{A^2(2-A)^2\lambda}{4x^6} + \dots , \quad (18)$$

where A and V are two constants of integration, referred to as the mass parameter and the velocity parameter, respectively. This is called the large-x asymptotic solution that is the form taken by all isothermal MHD (shock) solutions as they reach the region with sufficiently large x of the solution space.

The central MHD free-fall collapse for $x \to 0_+$ and $v, \alpha \to \infty$ corresponds to the asymptotic MHD solution[5]:

$$v(x) = -\left(\frac{2m_0}{x}\right)^{1/2} - \frac{3}{4}\sqrt{\frac{2x}{m_0}}\ln x - 2Lx^{1/2} + \dots , \quad (19)$$

$$\alpha(x) = \left(\frac{m_0}{2x^3}\right)^{1/2} - \frac{3}{8}\sqrt{\frac{2}{xm_0}}\ln x - Lx^{-1/2} + \dots , \quad (20)$$

$$b^2(x) = \frac{m_0\lambda}{2x} + \dots , \quad (21)$$

where m_0 is a constant standing for the central accretion rate and L is also a constant.

The central LP-type MHD asymptotic solution as $x \to 0_+$ is worked out by taking Taylor expansions of v and α in the MHD ODEs (12) and (13), under the assumption that $v \propto x$ and $\alpha \to D$, viz.

$$v(x) = \frac{2}{3}x + \frac{1}{5}\left(\frac{2}{27} - \frac{D}{9} - \frac{2D\lambda}{3}\right)x^3 + \dots , \quad (22)$$

$$\alpha(x) = D + \frac{1}{2}\left(\frac{2D}{9} - \frac{D^2}{3} - 2D^2\lambda\right)x^2 + \dots , \quad (23)$$

$$b^2(x) = \lambda D^2 x^2 + \dots , \quad (24)$$

where D is an integration constant called the central reduced density parameter.

The novel MHD asymptotic solution as $x \to 0_+$ that exists only when the magnetic field is strong enough ($\lambda > 4$) takes the form (Yu et al. 2006)

$$v(x) = Hx + \dots , \quad (25)$$

$$\alpha(x) = Kx^{-\eta} + \dots , \quad (26)$$

where K is a constant, while H and η are solved by substituting expressions (25) and (26) into the MHD ODEs (12) and (13)[6] to be

$$H = \frac{1}{2}\left[2 - \lambda \pm \left(\lambda^2 - 4\lambda\right)^{1/2}\right] < 0 , \quad (27)$$

$$\eta = \frac{1 - H + 2\lambda}{\lambda} , \quad \text{with} \quad 2 \leq \eta \leq 3 . \quad (28)$$

Then we have

$$b^2(x) = \frac{K^2\lambda}{x^{2(\eta-1)}} + \dots \quad (29)$$

As for the MHD solutions smoothly across the MSCL, we need to know the v' and α' at the very point x_* on the MSCL and take integrations from another point $x_* + dx$ immediately next to x_* with the asymptotic solution $v(x_* + dx) = v(x_*) + v' \cdot dx$, $\alpha(x_* + dx) = \alpha(x_*) + \alpha' \cdot dx$ as the approximated initial condition. $v(x_*)$ and $\alpha(x_*)$ are given by equations (14), together with $F_x = 0$. Here we note $v(x_*)$ as v, $\alpha(x_*)$ as α, and x_* as x, for short. The first two 1-order derivatives v' and α' are calculated from the following equations by the L'Hospital's rule (see Appendix B for their derivations):

$$\left[(v-x) - \frac{x\lambda}{(v-x)^2}\right](v')^2 + (x-v)v' - \frac{v}{x^2} = 0 , \quad (30)$$

$$\alpha' = \frac{2}{x}\left[\frac{v'}{(x-v)^2} - \frac{2}{x(x-v)}\right] . \quad (31)$$

The two roots of quadratic equation (30) correspond respectively to two types of possible solutions named Type 1 and Type 2 eigensolution across the MSCL, since given v', α' is completely determined from equation (31). We follow the definition of Yu et al. (2006) that the eigensolution with a smaller absolute value of v' belongs to Type 1 as the 'secondary direction', while that with a larger belongs to Type 2 as the 'primary direction'. It is known that such eigensolutions may be unstable. To be more concrete, from the perspective of numerical integrations, unstable eigensolutions

---

[5] For the leading terms, equation (10) reduces to $\alpha v' + v\alpha' + 2v\alpha/x = 0$, and equation (11) reduces to $vv' = \alpha v$, which leads to $v\alpha = -m_0/x^2$, knowing that $m \sim -x^2 v\alpha$ (as $x \to 0_+$ and $v, \alpha \to \infty$) from equation (9).

[6] This time, MHD ODEs (12) and (13) are simplified by $F_x \to -\lambda\alpha x^2$, $F_v \to (x-v)^2\alpha$, and $F_\alpha \to (x-v)\alpha^2 + 2\lambda x\alpha^2$.

across the MSCL are likely to hit the MSCL again with an improper choice of dx, in which case the singularities of MHD ODEs (12) and (13) may cause oscillations near the MSCL and the properties of the solutions when they finally 'escape' from the unstable region near the MSCL are unpredictable. Analytical explanations of the stability of eigensolutions across the MSCL can be found in Appendix A of Yu & Lou (2005), according to whose analysis, for a point x (i.e. x_*) within the range of $0 < x < \sqrt{1+2\lambda}$ [7] (as a saddle point), eigensolutions are stable , while for a point within the range of $\sqrt{1+2\lambda} < x < +\infty$ (as a nodal point), the primary direction is unstable, and the secondary direction is neutral stable. The properties of solutions crossing the MSCL depend crucially on the sign and magnitude of dx. In this paper, we only use Type 1 eigensolutions because they are always (at least neutral) stable, and the values of dx are chosen carefully to be small enough with specific signs for the accuracy and expected solution properties considerations.

3   PERPENDICULAR ISOTHERMAL MHD SHOCK CONDITIONS

We only consider the simplest isothermal MHD shock waves, in which case the velocities of both the isothermal MHD shock front and the gas are perpendicular to the traverse magnetic field. In the shock co-moving framework of reference, the physical variables of both sides of the isothermal MHD shock (ρ_1, u_1, B_1, p_1) and (ρ_2, u_2, B_2, p_2) are connected by the following equations for conservation of mass, momentum and magnetic flux (Yu et al. 2006):

$$\rho_2 u_2 = \rho_1 u_1 \ , \tag{32}$$

$$p_2 + B_2^2/(8\pi) + \rho_2 u_2^2 = p_1 + B_1^2/(8\pi) + \rho_1 u_1^2 \ , \tag{33}$$

$$B_2 u_2 = B_1 u_2 \ . \tag{34}$$

These isothermal MHD shock equations enable us to calculate (ρ_2, u_2, B_2, p_2) from (ρ_1, u_1, B_1, p_1) . We further define $M_1 \equiv u_1/a_1$ and $\beta_1 \equiv 8\pi p_1/\left(B_1^2\right) = 2a_1^2/v_{A1}^2$.

It is necessary to point out that unlike previous studies regarding polytropic gas (Lou & Gao 2006; Wang & Lou 2008), here we do not include the equation for (dynamical) MHD energy conservation across the shock front

$$\frac{\rho_2 u_2^3}{2} + \frac{\gamma p_2 u_2}{\gamma - 1} + \frac{B_2^2 u_2}{4\pi} = \frac{\rho_1 u_1^3}{2} + \frac{\gamma p_1 u_1}{\gamma - 1} + \frac{B_1^2 u_1}{4\pi} \ , \tag{35}$$

because it is of less significance in our isothermal model. We have already assumed that different parts (which are not separated by shocks) of the system share the same invariant temperature, which implies that heat conduction may be efficient in our model. Thus, it should be allowed that non-zero heat flux exists across the front shock, so that MHD energies (per unit mass) of the two sides of the shock front can be different. Actually, equation (35) is based on the presupposition that gas around the shock layer experience an 'isentropic' process, i.e. $\partial S/\partial t + \mathbf{u} \cdot \nabla S = \partial S/\partial t + u\partial S/\partial r = 0$, in which there is no heat flux, and that is why we use the

---

qualifier 'dynamical'. The general form of equation (35) with heat flux will be

$$\frac{\rho_2 u_2^3}{2} + \frac{\gamma p_2 u_2}{\gamma - 1} + \frac{B_2^2 u_2}{4\pi} + F_2$$
$$= \frac{\rho_1 u_1^3}{2} + \frac{\gamma p_1 u_1}{\gamma - 1} + \frac{B_1^2 u_1}{4\pi} + F_1 \ , \tag{36}$$

where $F_i = -\kappa_i \nabla T_i$ is the heat flux, κ_i is the coefficient of heat conduction, T_i is the temperature ($i = 1, 2$), and the equation for 'isentropic' condition becomes $\rho T \left(\partial S/\partial t + \mathbf{u} \cdot \nabla S\right) = \nabla \cdot (\kappa \nabla T)$. If there is no heat source within the shock layer, we must have $F_1 + F_2 = 0$. The values of F_1 and F_2 would not be calculated explicitly in our work, and they are just consistent with the results from equation (32)-(34).

Note that, when $\gamma \to 1$, equation (35) is badly formulated because the terms involving $1/(\gamma - 1)$ are problematic. Through comparison with the generalized version of the MHD shock conditions in our model, i.e. the MHD shock condition in the quasi-spherical MHD model of a general polytropic magneto-fluid (Wang & Lou 2008), we can show that in our model, if the effective entropy is conserved, we must have $\gamma \to 1$, and only one-temperature isothermal MHD shocks conserve (dynamically) MHD energy, while two-temperature shocks break (dynamical) MHD energy conservation (see Appendix D for details). The point here is that the isothermal MHD shocks in this paper must be accompanied by some processes (e.g. heat conduction, chemical reaction, nuclear fusion, and radiation transfer) that alter the MHD energies of both sides of the shock front, unless $\gamma \to 1$ and we are dealing with one-temperature isothermal MHD shocks.

3.1   The one-temperature isothermal MHD shock condition

For the one-temperature case, in which $a_1 = a_2$, the results are

$$u_1/u_2 = B_2/B_1 = p_2/p_1 = \rho_2/\rho_1 = X \ , \tag{37}$$

where X is a positive root of the quadratic equation (see appendix C for the derivation):

$$f_I(X) = X^2 + (\beta_1 + 1)X - \beta_1 M_1^2 = 0 \ . \tag{38}$$

This equation has only one positive root for X of physical sense.

By now, it is not determined whether the downstream properties are given or the upstream properties are given, so we use the notation (i, j) to obtain general expressions. $(i, j) = (d, u)$ means that the downstream properties are known, while $(i, j) = (u, d)$ the upstream. With the self-similar MHD transformation and the above formulae (37), we have

$$u_2 = u_j - u_s \ , \qquad u_1 = u_i - u_s \ ,$$
$$u_i = a_i v_i \ , \qquad u_j = a_j v_j \ ,$$
$$a_1 = a_i \ , \qquad a_2 = a_j \ , \tag{39}$$
$$u_s = a_i x_{si} = a_j x_{sj} \ , \qquad X = \rho_2/\rho_1 = \rho_j/\rho_i \ ,$$

where $u_s = dr_s/dt$ (r_s is the position of the shock front) is the speed of the isothermal MHD shock front. Note that all physical isothermal MHD (shock) solutions are restricted

---

[7] $\sqrt{1+2\lambda}$ is the intersection point of the MSCL and the x axis in the $-v$ versus x diagram (, i.e. $v = 0$).

in the upper-right region with respect to the straight line $x - v = 0$ in the $-v$ versus x plane, i.e. we always have $x - v > 0$. Therefore, it turns out that $u_1 = u_i - u_s = a_i(v_i - x_{si}) < 0$, which means that in the region before the shock (i.e. upstream: $i = u$), the gas flows relative to the shock front in a direction anti-parallel to the propagation direction of the shock (i.e. $-\hat{r}$ after the time-reversal operation), so the gas in this region enters the shock front as the shock propagate into it, that is why we call it the *front side*. Similarly, we can show that in the region after the shock (i.e. downstream), the gas leaves the shock front as the shock moves forward, that is why it is called the *back side*.

Besides, we have $a_i = a_j = a$, $x_{si} = x_{sj} = x_s$ for the one-temperature isothermal MHD shock case, then we arrive at the following expressions for the relations among self-similar dimensionless variables:

$$X = \alpha_j/\alpha_i = (v_i - x_s)/(v_j - x_s) ,$$
$$M_1 = v_i - x_s , \qquad \beta_1 = 2/(\lambda x_s^2 \alpha_i) . \tag{40}$$

Physically, we require that the upstream flow speed relative to the shock speed must exceed the upstream fast magneto-sonic speed, i.e. $a^2(v_u - x_s)^2 > a^2 + v_{Au}^2$. This requirement is consistent with the natural requirement for shock propagation that the upstream flow speed must exceed the downstream flow speed in the shock co-moving coordinates (Landau & Lifshitz 1987), i.e. $u_u - u_s > u_d - u_s$.

When $(i, j) = (u, d)$, since $v_A/a = \sqrt{\lambda \alpha} \cdot x$, the aforementioned requirement is equivalent to $f_I(X = 1) < 0$, that is to say, $M_1^2 > 1 + 2/\beta_1$, which further means that the positive root of equation (38) $X > 1$. And $X > 1$ is exactly the natural requirement for shock propagation as $(i, j) = (u, d)$ (see formulae (37), (39) and (40)).

While if $f_I(X = 1) > 0$, i.e. $M_1^2 < 1 + 2/\beta_1$, and we have the positive root $X < 1$, the case that $(i, j) = (u, d)$ is ruled out. Therefore, $(i, j) = (d, u)$ is necessary to ensure that the equivalent form of the above requirement becomes $M_2^2 > 1 + 2/\beta_2$ (and $X < 1$), where the definitions of M_2 and β_2 are similar to those of M_1 and β_1, i.e. $M_2 \equiv u_2/a_2 = M_1/X$ and $\beta_2 \equiv 8\pi p_2/(B_2^2) = \beta_1/X$. Note that $X < 1$, it is easily shown by formulae (40) and quadratic equation (38) that the requirement is met: $M_2^2 = M_1^2/X^2 = (1 + 1/X)/\beta_1 + 1/X > 1 + 2X/\beta_1 = 1 + 2/\beta_2$.

To sum up, when $(i, j) = (u, d)$, we require that $X > 1$, and when $(i, j) = (d, u)$, we require that $X < 1$.

3.2 The two-temperature isothermal MHD shock conditions

For the two-temperature isothermal MHD shock case, we perform the self-similar MHD transformation to equations (32) and (33) by equations (39), which gives

$$\alpha_i(v_i - x_{si})a_i = \alpha_j(v_j - x_{sj})a_j , \tag{41}$$
$$a_i^2 \left[\lambda \alpha_i^2 x_{si}^2/2 + \alpha_i + \alpha_i(v_i - x_{si})^2 \right]$$
$$= a_j^2 \left[\lambda \alpha_j^2 x_{sj}^2/2 + \alpha_j + \alpha_j(v_i - x_{sj})^2 \right] . \tag{42}$$

Then following the definitions of M_1 and β_1, it can be shown by means similar to that of the last section that

$$\tau = a_j/a_i = x_{si}/x_{sj} , \quad M_1 = v_i - x_{si} , \quad \beta_1 = 2/(\lambda x_{si}^2 \alpha_i) ,$$
$$X = \alpha_j/\alpha_i = (v_i - x_{si})/[\tau(v_j - x_{sj})] , \tag{43}$$

where X is a positive root of the following cubic equation (see appendix C for the derivation):

$$f_{II}(X) = X^3 + \beta_1 \tau^2 X^2 - (1 + \beta_1 + \beta_1 M_1^2)X + \beta_1 M_1^2 = 0. \tag{44}$$

When $(i, j) = (u, d)$, we still require that $X > 1$, because by formulae (43), $X > 1$ simply means that $u_u - u_s > u_d - u_s$, where $u_u - u_s$ and $u_d - u_s$ are the upstream velocity and the downstream flow velocity relative to the shock front. This is a natural requirement for shock propagation (Landau & Lifshitz 1987). Meanwhile, from the (effective) entropy increase condition $s_d - s_u = 2\ln(a_d/a_u) = 2\ln\tau > 0$, we further require that $\tau > 1$.

It can be shown that when $\tau > 1$, the cubic equation (44) may have two positive roots both larger than 1, or have no real root larger than 1 (see Appendix C). In the former case, we regard the shock solutions constructed by applying the smaller $X > 1$ of these two valid roots as satisfying Type 1 two-temperature isothermal MHD shock condition, while the larger $X > 1$ Type 2, given the downstream information. In the latter case of no real roots, it is impossible to construct converging isothermal MHD shocks with given τ and x_{su}.

When $(i, j) = (d, u)$, for the same reason mentioned in the case of $(i, j) = (u, d)$, on the contrary, we require that $\tau < 1$ and $X < 1$. Then the cubic equation (44) has only one positive root smaller than 1 when $\tau < 1$ (see Appendix C). We call this simpler case in which information of the downstream is given as the ordinary two-temperature isothermal MHD shock condition, since it is the only condition used by Yu et al. (2006). Detailed derivations and analysis of the cubic equation (44) is included in appendix C.

Now we know that given properties of the upstream, we can calculate the properties of two different types of downstream by Type 1 and 2 two-temperature isothermal MHD shock condition, while given those of the downstream, we can obtain only one type of upstream by the so-called ordinary two-temperature isothermal MHD shock condition, which implies an interesting 'two to one' relation between the upstream and the downstream. Such a relation is not a sign of mistakes. We further verified that even with this 'two to one' feature, these shock conditions are indeed reversable, i.e. if we calculate two types of downstream from certain upstream, and than calculate two types of upstream from these two types of downstream individually, the results are exactly the same with the initial upstream that we use. As $\tau \to 1$, Type 1 two-temperature isothermal MHD shock condition tends to produce trivial results (i.e. $X \to 1$: no shock at all), while results of Type 2 two-temperature isothermal MHD shock condition reduce to those of the one-temperature isothermal MHD shock solution[8]. Numerical investigations show that the upstream side locates in the MHD

---

[8] A stochastic interpretation of this fact is that two vital effects or features of the isothermal MHD shock is compression and heating of the gas, of which the former is mainly embodied by one-temperature isothermal MHD shock condition and Type 2 two-temperature isothermal MHD shock condition, while the latter Type 1 two-temperature isothermal MHD shock condition when τ is small. For large τ near its upper bound, the two types of conditions become the same and the effects are mixed for each type.

supersonic region, i.e. the right upper region in the $-v$ versus x plane separated from the MHD subsonic region by the MSCL[9]. Immediately after the shock, the downstream side following Type 1 condition only locates in the supersonic region, while that following Type 2 conditions the subsonic region. Besides, given $x_*(u)$ and x_{su} (or x_{sd}), τ has an upper bound due to our isothermal MHD shock conditions, and at this very upper bound of τ, the two types of downstream coincide with each other and touch, interestingly, the MSCL, so they are always separated by the MSCL.

Finally, the complete picture is that given $x_*(u)$ and x_{su} (or x_{sd}), when τ decreases from its upper bound to 1, immediately after the shock, starting from the MSCL, the two types of downstream are increasingly separated, and the one that follows Type 1 two-temperature isothermal MHD shock condition becomes trivial when $\tau = 1$, while the one by Type 2 two-temperature isothermal MHD shock condition reduces to that of certain one-temperature isothermal MHD shock solution.

4 SELF-SIMILAR ISOTHERMAL MHD VOID SOLUTIONS

The MHD void solution occurs when the zero mass line (ZML) $x - v = 0$ is hit at certain point x_1 (called the void boundary), where the dimensionless density α drops from α_0 to 0. The region with $x < x_1$ corresponds to a void region in which α, v, m and b all vanish. Since a type of converging isothermal MHD Shocks in Lou & Shi (2014) is constructed from void solutions, it is necessary to attain the MHD version of these solutions before constructing pertinent converging isothermal MHD Shocks. For the case of a weak magnetic field, we set $\lambda = 0.1$.

To construct void MHD solutions, the void boundary x_1 as well as the meeting point x_m is chosen at first. Then we integrate from $x_1 = v(x_1)$ to x_m with different α_0 values, which produces different (v, α) pairs to form a locus in the v versus α phase diagram. Meanwhile, we also perform integrations from different x_*s on the MSCL to x_m as Type 1 eigensolutions to plot another locus in the phase diagram. The intersection point of the two loci is a (v, α) pair corresponding further to certain α_0 and x_*, which are parameters in demand for the construction of MHD void solutions. Usually, a series of diagrams are needed to obtain the values of α_0 and x_* precisely enough, given x_1 and x_m.

The aforementioned method is the velocity-density matching method first introduced by Hunter (1977) and widely used in the present paper. The main spirit of it is to match the results of two sides, i.e. outward integration from certain point x_a starting with certain type of asymptotic solution to a chosen meeting point x_m and another inward integration from certain point x_b starting with certain type of asymptotic solution to the same meeting point x_m, in the v versus α phase diagram. Different types of asymptotic solutions have different parameter sets, say S_a and S_b.

Table 1. Information of five MHD void solutions with $\lambda = 0.1$, where x_1 is the void boundary, x_* is the starting point for integrations of Type 1 eigensolutions, x_m is the meeting point for α versus v phase diagram matching, and $x_2 = 500.0$ for calculating approximately the values of the velocity and mass parameters V and A defined in the large-x asymptotic solution (16) and (17) as x approaching the infinity, i.e. $\lim_{x \to +\infty} v = V \approx v(x_2)$, $\lim_{x \to +\infty} \alpha x^2 = A \approx \alpha(x_2)x_2^2$. This is accurate enough if we only revserve three significant digits for the value of V and four for that of A. L is the MHD solution label.

x_1	x_*	α_0	V	A	L	x_m
0.85	2.5013	1.8004	2.31	5.583	v1	1.5
0.4	2.2313	2.8406	1.98	5.021	v2	0.7
0.04	2.1641	3.6487	1.89	4.870	v3	0.5
0.004	0.8705	3401	-0.548	1.418	v4	0.1
0.002	0.8711	3485	-0.546	1.420	v5	0.1

for the outward integration and the inward integration, respectively ($x_a \in S_a$ and $x_b \in S_b$)[10]. Only one parameter is left unspecified for each of S_a and S_b, and it serves as the independent variable that generates the locus of that side. From now on, for brevity, we would not describe this method in detail again, instead, when applying this method, we simply point out the types of asymptotic solutions used for inward and outward integrations, the meeting point x_m, the pre-specified parameters and the independent variables for the loci. Figure 1 is an example of the α versus v phase diagrams in constructing MHD void solutions.

We construct five (typical) MHD void solutions, whose information is summarized in Table 1, and their $-v$ versus x plots are shown in Figure 2.

5 SELF-SIMILAR CONVERGING ISOTHERMAL MHD SHOCK SOLUTIONS

Similar to outgoing isothermal MHD Shocks, in the new solution space, the upstream side (which comes from $x \to 0_+$ instead of $x \to +\infty$) locates in the MHD supersonic region, i.e. the right upper region in the $-v$ versus x plane separated from the MHD subsonic region by the MSCL. As a result, except some MHD free-fall collapse solutions, all upstream solutions must cross the MSCL at least once. This additional requirement limits the diversity of our converging isothermal MHD Shocks compared with outgoing isothermal MHD Shocks. For instance, we find that starting from the novel MHD asymptotic solution for high magnetic fields as delineated by formulae (25)-(28) near the origin (say, $x_0 = 10^{-50}$), the solution cannot cross the MSCL smoothly, whatever parameters we choose. Therefore, we are not able to construct isothermal converging MHD shock solutions involving such a type of asymptotic solutions.

Besides, as mentioned in Section 3.2, downstream obtained by Type 2 two-temperature MHD shock condition locates in the subsonic region, and it must cross the MSCL again to reach the region with large x, which means that only

---

[9] This fact can be regarded as the MHD counterpart of the outcome in a non-magnetised ideal gas that the shock front always moves with supersonic speed as observed from the *front side* (i.e. the upstream) (Courant & Friedrichs 1976).

[10] Note that if integrations from any side (outward or inward) involving shocks, parameters of the shock belong to the parameter set of that side.
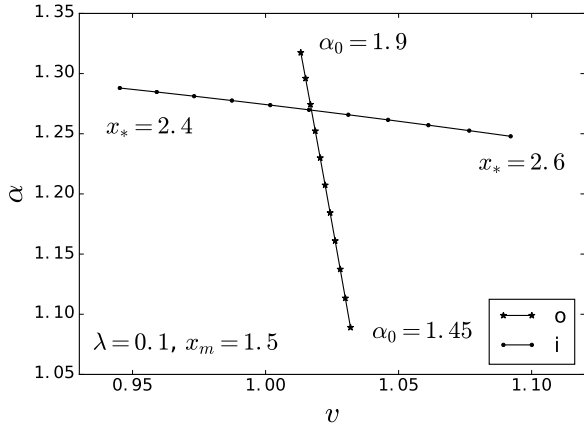
Figure 1. An example of the locus pair to construct MHD void solutions for illustration, where $\lambda = 0.1$, and the meeting point $x_m = 1.5$. The locus marked by asterisks comes from outward integrations (labelled by 'o') with a fixed void boundary $x_1 = 0.85$ and the dimensionless density at the void boundary α_0 varying in the range of $1.45 \sim 1.9$, while the locus marked by solid dots is produced by inward integrations (labelled by 'i') with different starting points x_*s on the MSCL in the range of $2.4 \sim 2.6$ as Type 1 eigensolutions.

Figure 2. The $-v$ versus x plots of five MHD void solutions, with $\lambda = 0.1$, whose information is contained in Table 1, and the curve labels are consistent with the MHD solution labels. The pertinent parameters are listed in the form of tuples, i.e. (the curve/MHD solution label L, the void boundary x_1, the dimensionless density at the void boundary α_0, the point at which the solution crosses the MSCL x_*): (v1, 0.85, 1.8004, 2.5013), (v2, 0.4, 2.8406, 2.2313), (v3, 0.04, 3.6487, 2.1641) and (v4, 0.004, 3401, 0.8705). The dash-dotted line corresponds to the zero mass line (ZML) $x - v = 0$. The dashed line is the magnetosonic critical line (MSCL).

one of the parameters x_{su} (or x_{sd}) and τ is adjustable due to the requirement of crossing the MSCL smoothly, while there is no such a confinement for downstream from Type 2 two-temperature MHD shock condition. The point here is that Type 2 two-temperature MHD shock condition gives less arbitrary results and it would not become trivial when reduced to the one-temperature case. In the light of this, the present study only uses Type 2 two-temperature MHD shock condition. In such a case, the properties of the downstream is completely determined by the position at which the upstream solution crosses the MSCL (just before it is shocked) and either of the position of the isothermal MHD shock (i.e. x_{su} or x_{sd}) or the strength of the shock τ.

The physical interpretations of the free-fall collapse solution and the EWCS are unclear (and even unrealistic) in the new solution space, though they can be used to construct isothermal MHD Shocks mathematically. We include the isothermal MHD shock solutions involving these asymptotic solutions (i.e. Class III isothermal MHD Shocks) in Appendix E. In the following subsections, we present the first two classes of converging isothermal MHD Shocks (characterised by MHD Larson-Penston (LP) type and converging MHD void asymptotic solutions) and twin converging isothermal MHD Shocks, which have different inner parts connected to different outer envelopes, whose velocity and density profile are characterised by the velocity and mass parameters V and A defined in the large-x solutoin (16) and (17).

5.1 Class I converging isothermal MHD shock solutions

Class I converging isothermal MHD Shocks are constructed by connecting shocked MHD LP-type solutions following
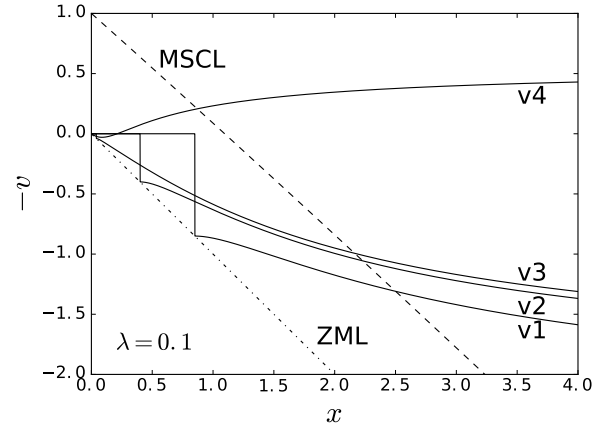
one-temperature or Type 2 two-temperature isothermal MHD shock condition with contracting envelopes under a weak magnetic field ($\lambda = 0.1$). To be more specific, for each of the three MHD LP-type solutions described in Yu & Lou (2005), knowing $x_*(1)$, with chosen x_{sd} and meeting point x_m, outward integrations (as Type 1 eigensolutions) from $x_*(1)$ shocked at certain x_{su} with different $\tau = x_{su}/x_{sd}$ values to x_m are taken, while inward integrations from different $x_*(2)$s on the MSCL to x_m as Type 1 eigensolutions are calculated, which leads to α versus v diagrams, one of which is shown in Figure 3, whose point of intersection denotes an isothermal MHD Shock. It is possible to construct many such solutions by choosing a variety of x_{su}s (see Section 6.1 for a guideline). However, for illustration, we only present three isothermal MHD Shocks for the three MHD LP-type solutions, respectively. Their information is contained in Table 2, while their properties portrayed by profiles of $v(x)$, $\alpha(x)$, $v_A(x)$, $b(x)$, and the reduced scaled density $R(x) = x^2 \alpha(x)/D$ are shown systematically in Figures 4-9.

5.2 Class II converging isothermal MHD shock solutions

The Class II converging isothermal MHD Shock is constructed by connecting the MHD void solution (presented in section 4) with the outer contracting envelope. The method is similar with that of constructing Class I converging isothermal MHD Shocks, while the inner parts (i.e. $0 < x < x_*(1)$) behind the outward integrations are delineated by MHD void solutions instead of MHD LP-type solutions, which produces α versus v loci as shown in Figure 10. Type 2 two-temperature isothermal MHD shock condition and Type 1 eigensolutions are applied to derive three such
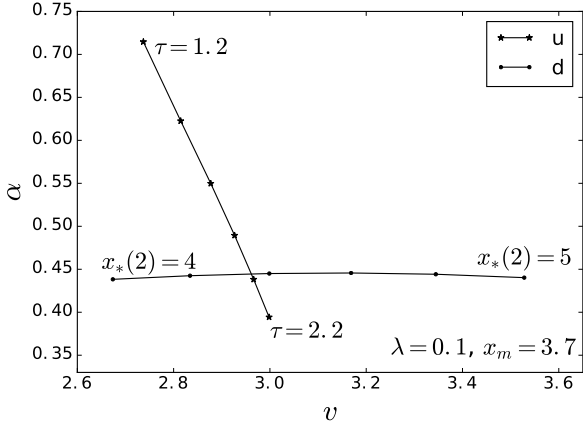
Figure 3. An example of the α versus v diagrams for constructing Class I converging isothermal MHD shocks, with $\lambda = 0.1$ and $x_m = 3.7$. The upstream locus (marked by asterisks, labelled by 'u') is formed by outward integrations starting from $x_*(1) = 2.16$ involving shocks at $x_{ud} = 3.5$ with different values of τ in the range of $1.2 \sim 2.2$. $x_*(1) = 2.16$ is where the MHD LP-type solution with the central density parameter $\ln D = 1.29$ crosses the MSCL. The downstream locus (marked by solid dot, labelled by 'd') is produced by inward integrations as Type 1 eigensolutions with different starting points $x_*(2)$s on the MSCL in the range of $4 \sim 5$.
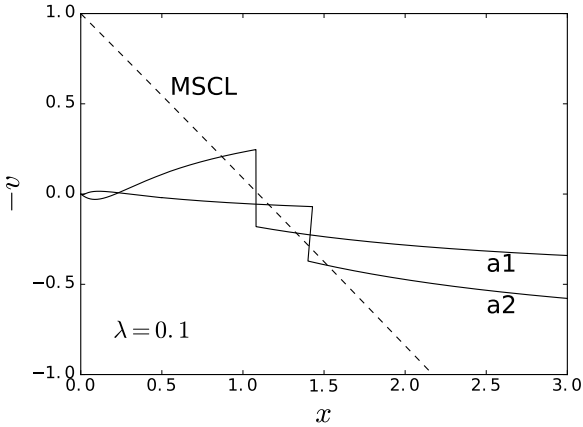
Figure 4. The $-v$ versus x diagram of the first two Class I converging isothermal MHD Shocks with $\lambda = 0.1$. The parameters of the pertinent inner MHD LP-type solutions and shock construction are listed in tuples (the curve/MHD solution label L, the central density parameter $\ln D$, the point at which the solution crosses the MSCL for the first time $x_*(1)$, the meeting point x_m): (a1, 8.15, 0.87, 1.25), (a2, 12.7, 1.16, 1.45). Information of these isothermal MHD shock solutions can be found in Table 2, since the curve labels here are consistent with the MHD solution labels. The dashed line corresponds to the MSCL.

Table 2. Class I converging isothermal MHD Shocks with $\lambda = 0.1$, where x_{su} is the upstream shock position (at which the values of v and α are known from outward integrations), x_{sd} is the downstream shock position (at which the values of v and α are calculated from those of the upstream side by one-temperature or Type 2 two-temperature isothermal MHD shock condition), $x_*(2)$ is the point at which the downstream integration crosses the MSCL, $\tau = x_{su}/x_{sd}$, and $x_2 = 500.0$ for calculating approximately the values of the velocity and mass parameters V and A. Values of the central reduced density parameter D for LP-type solutions involved, the starting points $x_*(1)$s on the MSCL and the meeting points x_ms are (L, $\ln D$, $x_*(1)$, x_m): (a1, 8.15, 0.87, 1.25), (a2, 12.7, 1.16, 1.45), (a3, 1.29, 2.16, 3.7), where L is the MHD solution label.

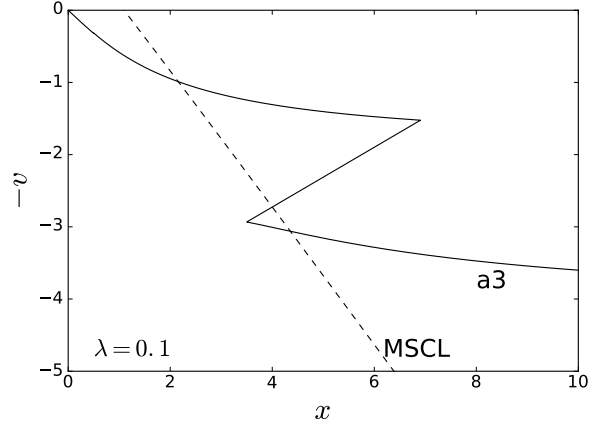| x_{sd}	x_{su}	$x_*(2)$	τ	V	A	L
1.08	1.08	1.3288	1	0.509	2.651	a1
1.4	1.4289	1.5226	1.0207	0.889	3.204	a2
3.5	6.9058	4.3552	1.9731	4.18	8.519	a3

Figure 5. The $-v$ versus x diagram of the third Class I converging isothermal MHD Shocks with $\lambda = 0.1$, in which for the inner MHD LP-type solution involved, the central density parameter $\ln D = 1.29$, the point at which the solution crosses the MSCL for the first time $x_*(1) = 2.16$, and the meeting point $x_m = 3.7$). Table 2 contains the information of the pertinent isothermal MHD Shock, whose MHD solution label is consistent with the curve label a3 here. The dashed line corresponds to the MSCL.

solutions whose information is shown in Table 3, and properties in Figure 11-13.

5.3 Twin converging isothermal MHD shock solutions

In this section we construct three twin converging isothermal MHD Shocks with three isothermal MHD shock solutions chosen from the results of constructed Shocks (i.e. a1, b1 and c6, see Appendix E for information of c6) as the upstream. The method remains the same, and Type 1 eigensolution is used to take the downstream integration. To avoid confusion with the notations of these already shocked upstream solutions, we note the starting point on the MSCL for the second isothermal MHD shock as $x_*(u)$ and the point at which the
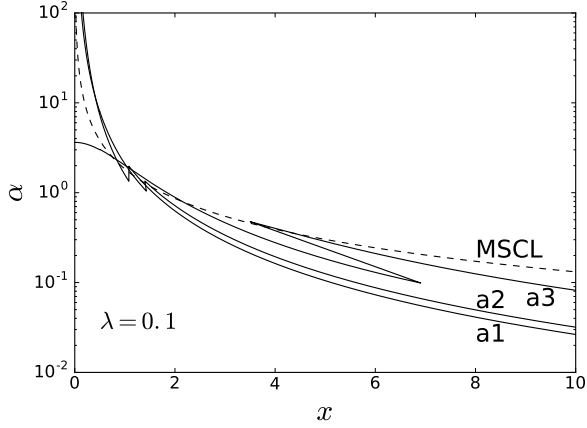
Figure 6. The α versus x diagram of Class I converging isothermal MHD Shocks with $\lambda = 0.1$, in which the α axis is in a logarithmic scale, and the curve/MHD solution labels (as well as parameters of the solutions) are consistent with those in Figures 4-5 and Table 2. The dashed line corresponds to the MSCL. It is shown that the shocks have compressed the gas as $\alpha(x_{sd}) > \alpha(x_{su})$.
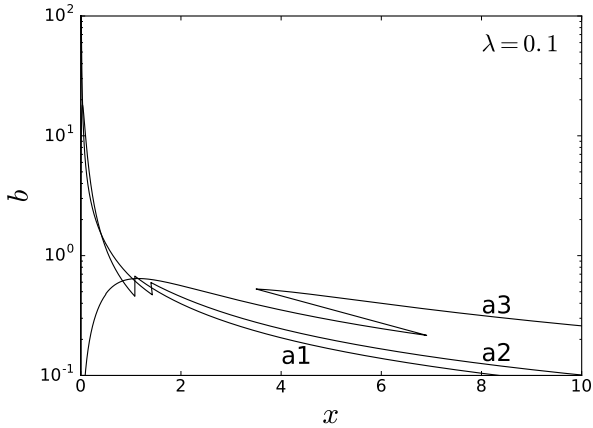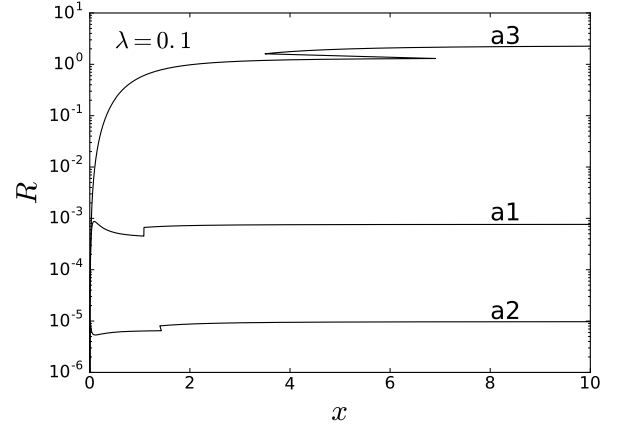

Figure 8. The R versus x diagram of Class I converging isothermal MHD Shocks with $\lambda = 0.1$, in which the R axis is in a logarithmic scale, and the curve/MHD solution labels (as well as parameters of the solutions) are consistent with those in Figures 4-5 and Table 2.
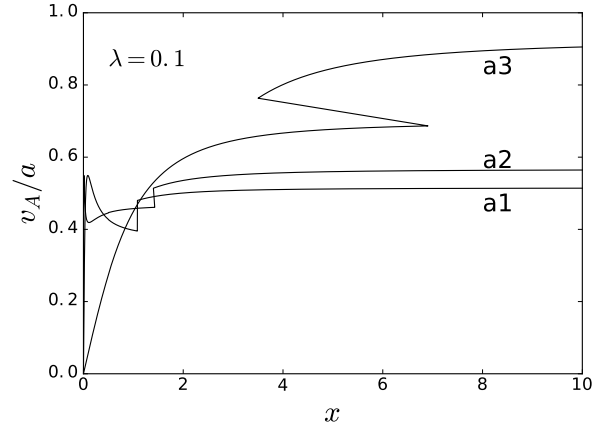

Figure 7. The b versus x diagram of Class I converging isothermal MHD Shocks with $\lambda = 0.1$, in which the b axis is in a logarithmic scale, and the curve/MHD solution labels (as well as parameters of the solutions) are consistent with those in Figures 4-5 and Table 2.

Figure 9. The v_A/a versus x diagram of Class I converging isothermal MHD Shocks with $\lambda = 0.1$, in which the curve/MHD solution labels (as well as parameters of the solutions) are consistent with those in Figures 4-5 and Table 2.

6 SUMMARY AND DISCUSSIONS

6.1 General guideline to the construction of converging isothermal MHD shock solutions

It is known from the above results that the upstream of any converging isothermal MHD Shock (found through α versus v phase diagrams) comes from certain point (which is referred as $x_*(u)$ for convenience) on the MSCL (as Type 1 eigensolutions), except for that in the Appendix E0.1, which implies general properties of their phase diagrams. That is to say, we may find by numerical trials a general empirical guideline to the construction of such isothermal MHD shock solutions.

For one-temperature isothermal MHD Shocks, as shown

twin converging isothermal MHD Shock crosses the MSCL for the last time as $x_*(d)$[11]. The information of these MHD solutions are shown in Table 4, and relevant parameters in Figure 14-15.

---

[11] Actually, it is $x_*(d)$ and the type of eigensolution that determine the properties of the outer envelope (see Section 6.1 and Figure 18).

Table 3. Class II converging isothermal MHD Shocks with $\lambda = 0.1$, where x_{sd} is the downstream shock position, x_{su} is the upstream shock position, $x_*(2)$ is the point at which the downstream integration crosses the MSCL , $\tau = x_{su}/x_{sd}$, and $x_2 = 500.0$ for calculating approximately the values of the velocity and mass parameters V and A. The void boundaries x_1s and values of the reduced density parameter α_0 for relevant MHD void solutions, the starting point $x_*(1)$s and the meeting points x_ms are (L, x_1, α_0, $x_*(1)$, x_m): (b1, 0.002, 3485, 0.8711, 1.3), (b2, 0.4, 2.8406, 2.2313, 4.2), (b3, 0.85, 1.8004, 2.5013, 4.7), where L is the MHD solution label.

x_{sd}	x_{su}	$x_*(2)$	τ	V	A	L
1.15	1.1611	1.4580	1.0097	0.766	3.020	b1
4.0	9.2979	4.9878	2.3245	4.79	9.357	b2
4.5	12.0048	5.5628	2.6773	5.33	10.08	b3
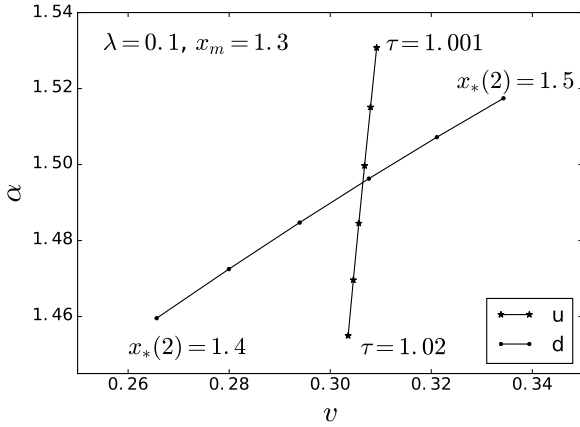
Figure 10. One pair of the α versus v loci in search of the Class II converging isothermal MHD Shock with $\lambda = 0.1$ and $x_m = 1.3$. The upstream locus (marked by asterisks, labelled by 'u') is formed by outward integrations starting from $x_*(1) = 0.8711$ involving shocks at $x_{ud} = 1.15$ with different values of τ in the range of $1.001 \sim 1.02$. $x_*(1) = 0.8711$ is where the MHD void solution with the void boundary $x_1 = 0.002$ and the dimensionless density $\alpha_0 = 3485$ at the void boundary crosses the MSCL. The downstream locus (marked by solid dot, labelled by 'd') is produced by inward integrations as Type 1 eigensolutions with different starting points $x_*(2)$s on the MSCL in the range of $1.4 \sim 1.5$.

Table 4. Three twin converging isothermal MHD shock solutions with $\lambda = 0.1$, where $x_*(d)$ is the point at which the solution crosses the MSCL for the last time, $x_2 = 500.0$ for calculating the values of the velocity and mass parameters V and A. The upstream MHD solution label n-L denotes that the upstream of the Shock corresponds to the MHD solution with label L in Table n.

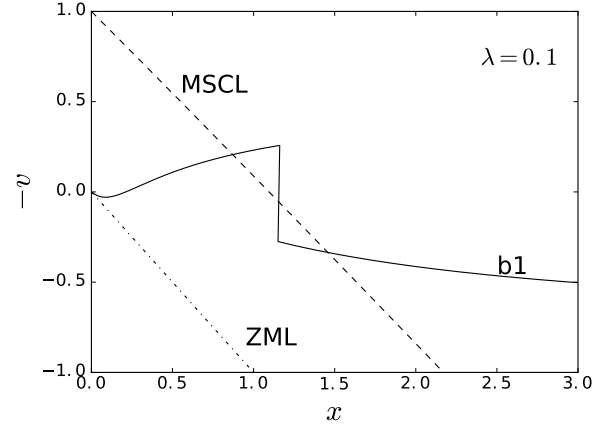| x_{sd}	x_{su}	τ	$x_*(d)$	V	A	n-L
2.0	2.3276	1.1638	2.4002	2.19	5.380	2-a1
2.5	3.4590	1.3836	3.1392	2.99	6.720	3-b1
2.7	3.9976	1.4806	3.3944	3.25	7.127	E3-c6

Figure 11. The $-v$ versus x diagram of the first Class II converging isothermal MHD Shock with $\lambda = 0.1$, in which for the inner MHD void solution involved, the void boundary $x_1 = 0.002$, the dimensionless density at the void boundary $\alpha_0 = 3485$, the point at which the solution crosses the MSCL for the first time $x_*(1) = 0.8711$, and the meeting point $x_m = 1.3$. Table 3 contains the information of the pertinent isothermal MHD Shock, whose MHD solution label is consistent with the curve label b1 here. The dashed line corresponds to the MSCL, and the dashed dotted line is the ZML $v - x = 0$.
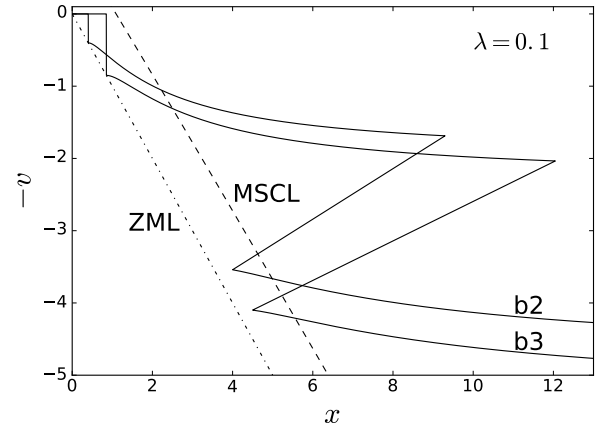

Figure 12. The $-v$ versus x diagram of the second and the third Class II converging isothermal MHD Shocks with $\lambda = 0.1$. The parameters of the pertinent inner MHD void solutions and shock construction are listed in tuples (the curve/MHD solution label L, the void boundary x_1, the dimensionless density at the void boundary α_0, the point at which the solution crosses the MSCL for the first time $x_*(1)$, the meeting point x_m): (b2, 0.4, 2.8406, 2.2313, 4.2), (b3, 0.85, 1.8004, 2.5013, 4.7). Information of these isothermal shock solutions can be found in Table 3. The dashed line corresponds to the MSCL, and the dashed dotted line is the ZML $v - x = 0$.
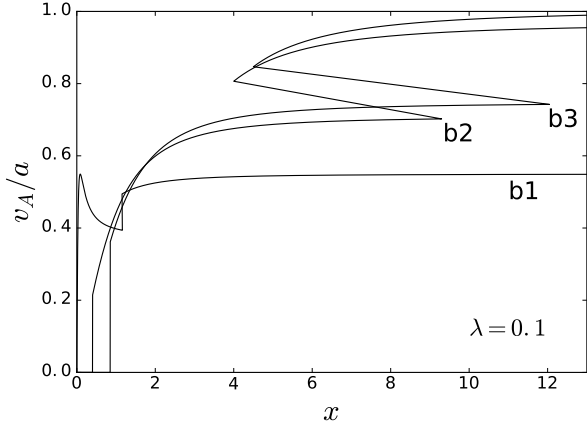
Figure 13. The v_A/a versus x diagram of Class II converging isothermal MHD Shocks with $\lambda = 0.1$, in which the curve/MHD solution labels (as well as parameters of the solutions) are consistent with those in Figures 11-12 and Table 3.
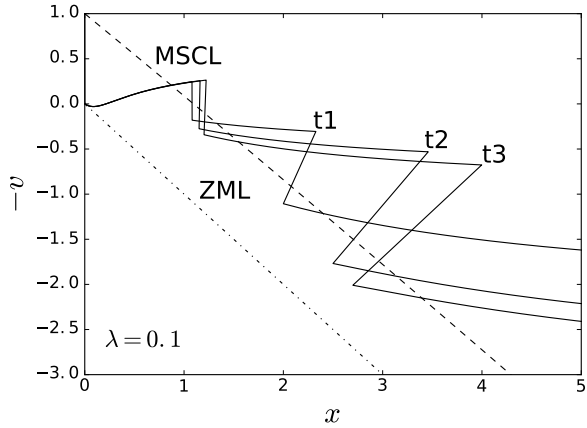

Figure 15. The v_A/a versus x diagram of twin converging isothermal MHD Shocks with $\lambda = 0.1$, corresponding to Figure 14 and Table 4.

Figure 14. The $-v$ versus x diagram of twin converging isothermal MHD Shocks with $\lambda = 0.1$ (the curve label, the upstream MHD solution label n-L, $x_*(u)$, x_m): (t1, 2-a1, 1.3288, 2.1), (t2, 3-b1, 1.4580, 2.7), (t3, E3-c6, 1.5500, 3.0). See Table 4 for more information. The dashed line corresponds to the MSCL.

in Figure 16, given x_m and $x_*(u)$, with different x_ss, in the α versus v phase plane, the locus of one-temperature upstream integrations is like a line with a positive slope which is always larger than the largest value (positive or negative) of the slope of (lines tangent to) the locus generated by downstream integrations with different $x_*(d)$s as the starting point, in the interested region (where downstream locus and upstream locus intersect with each other). Besides, for both the upstream locus and the downstream locus, the value of v increases as x_s and $x_*(d)$ increase. Therefore, in the case that the locus of one-temperature upstream is above that of downstream, it is possible to find a point of intersection as the values of v decreases for both locus, which denotes smaller x_s and $x_*(d)$, and vice versa. However, for
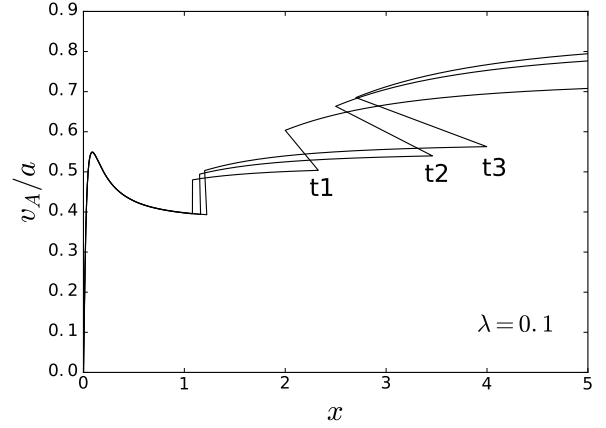
sufficient large $x_*(u)$, we cannot find an intersection of the one-temperature upstream locus and the downstream locus even until x_s shrinks back to $x_*(u)$, which means that there is no one-temperature isothermal MHD shock.

As for two-temperature isothermal MHD Shocks (under Type 2 two-temperature isothermal MHD shock condition), then chosen x_{sd} as well as x_m, by increasing the value of $\tau = x_{su}/x_{sd}$ from 1, we have the locus of two-temperature upstream going down from larger α to smaller α with positive or negative slope whose absolute value is much larger than that of the locus of one-temperature isothermal MHD Shocks. Actually, these locus of two-temperature isothermal MHD Shocks start from the locus of one temperature isothermal MHD shocks, in that the isothermal MHD shock reduces to one-temperature isothermal MHD shock when $\tau \to 1$, as shown in Figure 16 and 17. As a result, intersections can only be found when the locus of one-temperature upstream is above that of downstream. This is true for sufficiently large $x_*(u)$. Moreover, it is necessary to point out that given $x_*(u)$ and x_{sd}, τ has an upper bound due to the isothermal MHD shock condition. This upper bound grows larger as x_{sd} increases. Figure 16 and 17 as well as other locus diagrams also indicate that for certain $x_*(u)$, as both x_{sd} and $x_*(d)$ increase, the separation of the starting point of the two-temperature upstream locus with possible intersection point on the downstream locus becomes greater. Since the two-temperature upstream locus goes down by the rising upper-bound of τ with a speed higher than the rate of the increase of separation between the downstream locus and the one-temperature upstream locus, due to the increase of x_{sd} as well as $x_*(d)$, we need larger x_{sd} when the upper-bound of τ is not large enough for the two-temperature upstream locus to reach the downstream locus. Thus, given $x_*(u)$, a sufficiently large x_{sd} is in demand to make an intersection of the two-temperature upstream locus and the downstream locus possible. The larger the x_{sd} the larger the τ at the intersection point and the larger the corresponding $x_*(d)$. If $x_*(u)$ is not sufficiently large, there is also a lower bond of x_{sd} which corresponds exactly to the intersection point of the one-temperature upstream locus and the downstream locus.
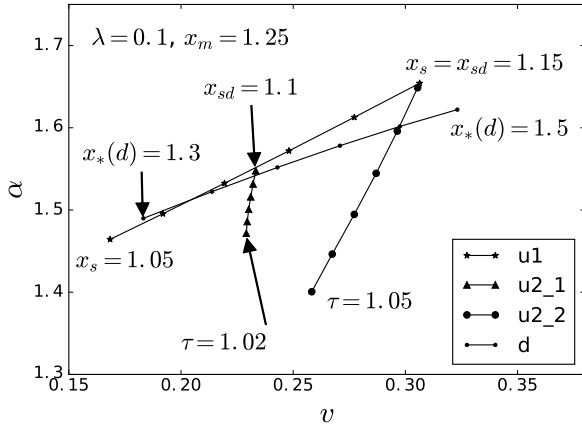
Figure 16. A typical phase diagram where an one-temperature isothermal MHD shock can be found with $\lambda = 0.1$, $x_m = 1.25$ and $x_*(u) = 0.87 < \sqrt{1.2} = \sqrt{1 + 2\lambda}$. The downstream locus ('d'), one-temperature upstream locus ('u1'), two-temperature upstream locus 1 ('u2_1') and two-temperature upstream locus 2 ('u2_2') are marked by solid dots, asterisks, triangles and solid circles, respectively. For any two-temperature upstream locus, x_{sd} is annotated at the its starting point on the one-temperature upstream locus, while the approximate upper bond of τ are annotated at the end.
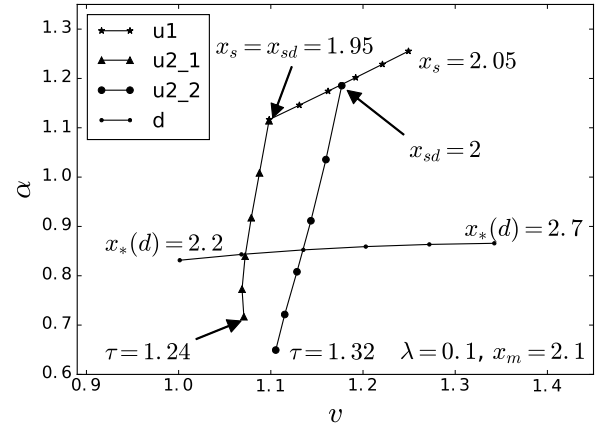

Figure 17. A phase diagram in search of two-temperature isothermal MHD shocks with $\lambda = 0.1$, $x_m = 2.1$ and $x_*(u) = 1.3288 > \sqrt{1.2} = \sqrt{1 + 2\lambda}$. The downstream locus ('d'), one-temperature upstream locus ('u1'), two-temperature upstream locus 1 ('u2_1') and two-temperature upstream locus 2 ('u2_2') are marked by solid dots, asterisks, triangles and solid circles, respectively. For any two-temperature upstream locus, x_{sd} is annotated at the its starting point on the one-temperature upstream locus, while the approximate upper bond of τ are annotated at the end.

In summary, when constructing two-temperature isothermal MHD shocks (in search of $x_*(d)$ and τ), there is a lower bond of x_{sd} which becomes larger as the value of $x_*(u)$ rises, and the final τ at the intersection point as well as $x_*(d)$ increases as x_{sd} increases for any given $x_*(u)$. It is also shown in Table 1-4 that given λ, the values of the velocity parameter V and the mass parameter A for large x approaching the infinity are completely determined by $x_*(d)$ where the solution crosses the MSCL for the last time, and both V and A values increase as $x_*(d)$ increases. We also find by numerical explorations that for integrations from the same starting point x_* at the MSCL/SCL to certain large x_2 where $v(x_2)$ and $\alpha(x_2)$ take approximately the asymptotic form of equation (16) and (17), the values of both V and A are smaller in MHD models than those in the pure HD model as presented in Figure 18.

To be more precise, the analysis above is limited in the case that $\lambda = 0.1$ and the chosen meeting point x_m is not too close to the origin. It is possible to evaluate the limitation of these conclusions in detail with further numerical explorations. Actually, the properties of the downstream locus formed by the results of backward integrations from different $x_*(d)$s (as Type 1 eigensolutions) are determined by the parameter λ and the meeting point x_m. Generally speaking, the downstream locus has two 'turning region (point)' (see Figure 19 and 20) which can be understood by the following delineations. Given certain x_m, there is a very λ_c. When $\lambda > \lambda_c$, v is always an increasing function with respect to $x_*(d)$, and at the first turning region (point), $\alpha(v)$ shifts from an increasing function to a decreasing function. While $\lambda < \lambda_c$, as $x_*(d)$ increases, v increases, except in a region (the first turning region), which leads to the 'inward bending' of the locus, since α decreases as v decreases in this
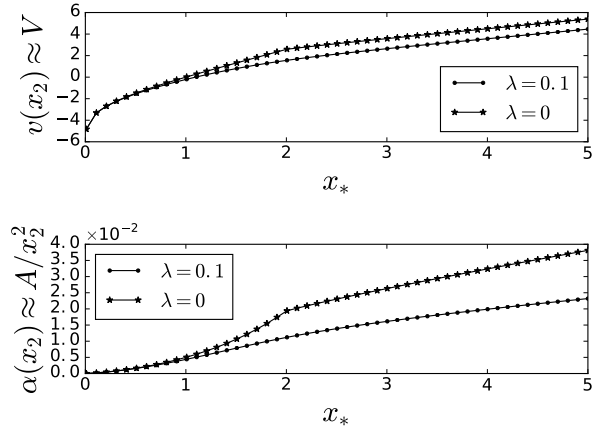

Figure 18. The $v(x_2)$ versus x_* diagram (upper panel) and the $\alpha(x_2)$ versus x_* diagram (lower panel) for the MHD model with $\lambda = 0.1$ and the HD model with $\lambda = 0$, where x_* is the starting point of the Type 1 eigensolution, and $x_2 = 20.0$ is the ending point for evaluating values of the velocity and mass parameters V and A as $v(x_2) \approx V$ and $\alpha(x_2) \approx A/x_2^2$. It is shown that the values of both V and A are smaller in the MHD model than those in the HD model. Besides, different from the case of the MHD model, there is an obvious tuning point $x_* = 2$ on the curve of $v(x_2)$ or $\alpha(x_2)$ in the HD model, which has the same nature as the second turning points in Figure 20, i.e. due to the definition of the two types of eigensolutions (see Footnote 12 for details).
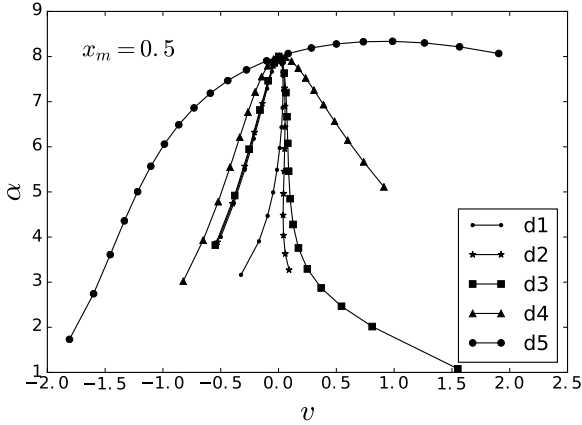
Figure 19. Examples of downstream loci with different λ values and the same meeting point $x_m = 0.5$ (label, marker, λ, starting $x_*^s(d)$, ending $x_*^e(d)$): (d1, solid dot, 0, 0.5, 1.75), (d2, asterisk, 0.06, 0.5, 2.0), (d3, square, 0.1, 0.5, 2.5), (d4, triangle, 1, 0.5, 3.0), (d5, solid circle, 10, 0.5, 7.0). Through numerical trails (which are not shown here), we find that $0.07 < \lambda_c < 0.08$ for $x_m = 0.5$.

Figure 20. Examples of downstream loci with different λ values and the same meeting point $x_m = 1.0$, starting $x_*^s(d) = 1.0$ and ending $x_*^e(d) = 2.5$ (label, marker, λ): (d1, solid dot, 0), (d2, asterisk, 5×10^{-4}), (d3, triangle, 2×10^{-3}), (d4, solid circle, 0.01). It is shown that $2 \times 10^{-3} < \lambda_c < 0.01$ for $x_m = 1.0$, which is smaller than that for $x_m = 0.5$, and the corresponding $x_*(d)$ for the second turning point increases as λ increases, while the sharpness of the 'turning' lowers down.

case. The larger the λ, the smaller the first turning region, and when λ exceeds λ_c, the first turning region shrinks to a point, which enables us to define a monotropic function $\alpha(v)$. During the 'inward bending' stage, it is of likelihood that the integration hits the MSCL/SCL for larger $x_*(d)$, in that v decreases as $x_*(d)$ increases. This is exactly the case that $\lambda = 0$ and $x_m = 0.5$, where the SCL is hit for certain $x_*(d)$ in the range of $1.8 \sim 1.9$. If this does not happen, we come to the second turning point[12] around which the 'inward bending' region ends for $\lambda < \lambda_c$, or the derivative of $\alpha(v)$ with respect to v becomes larger for $\lambda > \lambda_c$. The corresponding $x_*(d)$ for the second turning point increases as λ increases and the sharpness of the 'turning' lowers down. Besides, after the second turning point, there could be another upper bond for $x_*(d)$, where the backward integration hits the ZML $v = x$. Numerical results further shows that λ_c decreases when x_m becomes larger and the instruction proposed in the last two paragraphs can be applied to the case in which $\lambda > \lambda_c$.

Another overall view on converging isothermal MHD shock solutions is that the consequence of the isothermal MHD shock is a larger $x_*(d) > x_*(u)$ at which the solution crosses the MSCL for the last time. As a result, if we con-

sider the properties at large x, i.e. $t \to 0_-$, or $r \to +\infty$, the parameter for the velocity of this final or outer envelope $\lim\limits_{x \to +\infty} \tilde{v} = -V$ decreases, while the parameter for the reduced density $\lim\limits_{x \to +\infty} x^2\alpha = A$ increases, due to the (contracting) isothermal MHD shock (see Figure E1 and Table E1 for examples). If $-V$ varies from a positive value to a negative value after the isothermal MHD shock, the outer envelope changes from an expanding one to a contracting one, which indicates that for certain state $x \to 0_+$ in the early stage of evolution ($t \to -\infty$) or near the center ($r \to 0$) related to an expanding outer envelope, it is possible to connect it with a contracting outer envelope by an isothermal MHD shock. And for a state matched with a contracting outer envelope, it is possible to enhance the speed as well as density of the outer envelope by an isothermal MHD shock. The static envelope is also alterable and accessible in this way.

6.2 Astrophysical applications

6.2.1 Converging isothermal MHD shocks for protostar formation

Magnetic fields can play important roles in forming protostars. Simulations of the gravitational collapse in MHD turbulent molecular clouds by Heitsch et al. (2001) indicates that magnetic fields can support the molecular clouds magneto-statically preventing it from collapse (subcritical), or merely delay and weaken the collapses of them (supercritical). Our converging isothermal MHD shock solutions do not correspond to the whole collapse process, however, can serve as the collapse-triggering mechanism related to the latter case, since the magnetic field in our quasi-spherically symmetric model is travese and random (which contributes

---

[12] This turning point is due to the definition of the two types of eigensolutions. Given λ, if the soltion crosses the MSCL/SCL at x_*, the quadratic equation (30) have two roots which can be expressed explicitly by $x = x_*$ and $v = v(x_*)$. Since $v(x_*)$ is a function of x_*, these two roots are also functions of x_* as $v'_+(x_*)$ and $v'_-(x_*)$. If there is a very x_*^t for $|v'_+(x_*^t)| = |v'_-(x_*^t)|$, as Type 1 eigensolution has the smaller absolute value of v' at the MSCL, its initial condition may vary following different functions (i.e. $v'_+(x_*)$ or $v'_-(x_*)$) with respect to x_* before and after x_*^t. If so, for a parameter involving Type 1 eigensolutions (e.g. v and α at certain meeting point x_m calculated by integrations starting from the MSCL/SCL as Type 1 eigensolutions), a turning point would occur in the relevant parameter space corresponding to x_*^t.
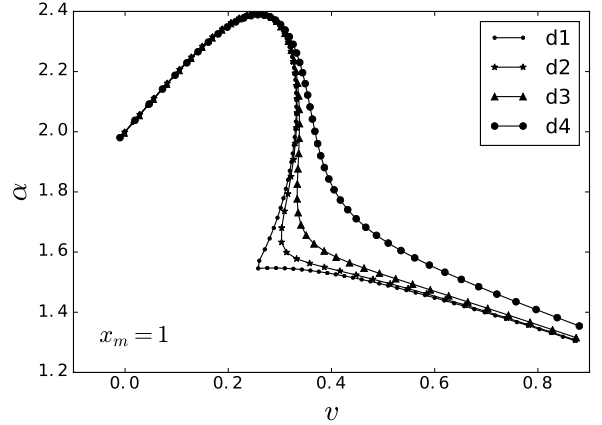
only magnetic pressure and tension force terms). Consider a quasi-spherical magnetised molecular cloud in a critical state which tends to collapse and form a core, a converging isothermal MHD shock can be generated by circumstance fluctuations (e.g. motions of gas triggered by outgoing shocks from nearby supernovae) and propagate towards the center, resulting in (turbulent) density enhancement and inward flow speed behind it, which causes further gravitational core collapse of the molecular cloud.

For such a grossly spherical magnetised molecular clouds with a size $\sim 0.29 - 0.39$ pc (Klessen 2001), the following parameters feature its properties:

$$t_{ff} = \sqrt{\frac{3\pi}{32G\rho_0}}$$
$$\sim 1.16 \times 10^6 \text{ yr} \left(\frac{n}{10^3 \text{ cm}^{-3}} \frac{\mu}{m_{H2}}\right)^{-1/2}, \quad (45)$$

$$\lambda_J = a\sqrt{\frac{\pi}{G\rho_0}} \sim 0.77 \text{ pc}$$
$$\times \left(\frac{a}{0.2 \text{ km} \cdot \text{s}^{-1}}\right) \left(\frac{n}{10^3 \text{ cm}^{-3}} \frac{\mu}{m_{H2}}\right)^{-1/2}, \quad (46)$$

$$B = \sqrt{8\pi\rho_0 a^2 \frac{1}{\beta}} \sim 5.77 \ \mu\text{G}$$
$$\times \left(\frac{a}{0.2 \text{ km} \cdot \text{s}^{-1}}\right) \left(\frac{n}{10^3 \text{ cm}^{-3}} \frac{\mu}{m_{H2}} \frac{1}{\beta}\right)^{1/2}, \quad (47)$$

where t_{ff} is the free-fall time, λ_J is the Jean's length, B is an estimated magnetic field with β as a dimensionless parameter characterising its strength (i.e. the ratio of the thermal pressure $p_{th} = a^2\rho_0$ and the magnetic pressure $p_m = B^2/(8\pi)$), ρ_0 is the mean mass density of the molecular cloud, n is the mean molecule number density, μ is the average mass of one molecule, $m_{H2} = 3.32 \times 10^{-24}$ g is the mass of a hydrogen molecule, $a = (k_BT/\mu)^{1/2}$ is the isothermal sound speed with the Boltzmann constant $k_B = 1.381 \times 10^{-16} \text{ cm}^2 \cdot \text{g} \cdot \text{s}^{-2} \cdot \text{K}^{-1}$, T is the temperature, and $G = 6.67^{-8} \text{ cm}^3 \cdot \text{g}^{-1} \cdot \text{s}^{-2}$ is the universal gravitational constant.

To apply the Class I converging isothermal MHD shock solution to this cloud, we need to establish relations among the above parameters with self-similar variables. Assuming that the mass density is exactly ρ_0 at the centre initially as $t \to -\infty$, $r \to 0$, $x \to 0_+$, and $\alpha \to D$ for the MHD LP-type solution, the dynamic time scale t_0 of this MHD shock-collapse-triggering process, i.e. the time taken for the isothermal MHD shock to reach the centre can be speculated (from equations (7) for the self-similar MHD transformation) by

$$t_0 = \sqrt{\frac{D}{4\pi G\rho_0}}$$
$$\sim 6 \times 10^5 \text{ yr} \left(\frac{n}{10^3 \text{ cm}^{-3}} \frac{\mu}{m_{H2}}\right)^{-1/2} \sqrt{D}. \quad (48)$$

During the time interval $-t_0 \sim 0_-$, the shock front propagates towards the increasingly denser centre which forms the core of the protostar[13] and compresses the inflow gas. It

is natural to assume that the upstream (i.e. the inner part which has not been shocked yet) remains at temperature T and has a sound speed $a(= a_u = a_d/\tau)$, then the radius at which the isothermal MHD shock appears and the enclosed mass defined by this radius are

$$r_s = ax_{su}t_0 \sim 0.123 \text{ pc}$$
$$\times \left(\frac{a}{0.2 \text{ km} \cdot \text{s}^{-1}}\right) \left(\frac{n}{10^3 \text{ cm}^{-3}} \frac{\mu}{m_{H2}}\right)^{-\frac{1}{2}} x_{su}\sqrt{D}, \quad (49)$$
$$M_s = \frac{a^3 t_0}{G} m(x_{su}) \sim 1.14 \ M_\odot \left(\frac{a}{0.2 \text{ km} \cdot \text{s}^{-1}}\right)^3$$
$$\times \left(\frac{n}{10^3 \text{ cm}^{-3}} \frac{\mu}{m_{H2}}\right)^{-\frac{1}{2}} m(x_{su}) \sqrt{D}. \quad (50)$$

Behind the isothermal MHD shock, the outer envelope (i.e. $x \to +\infty$) is also contracting, whose speed and density profile may serve as indications for the rate and strength of the further core collapse process, which can be derived from the self-similar MHD transformation (7) together with the large-x asymptotic solution (16) and (17):

$$u = a_d\widetilde{v} = -a_d v \sim -a_d V = -aV\tau, \quad (51)$$
$$\rho = \frac{\alpha}{4\pi Gt^2} \sim \frac{Aa_d^2}{4\pi Gr^2} = \frac{a^2}{4\pi Gr^2} A\tau^2 \sim 477 \text{ g} \cdot \text{cm}^{-3}$$
$$\times \left(\frac{a}{0.2 \text{ km} \cdot \text{s}^{-1}}\right)^2 \left(\frac{r}{10^6 \text{ cm}}\right)^{-2} A\tau^2. \quad (52)$$

As for the magnetic field strength, we have to calculate the parameter λ defined in equation (6) from β. As a speculation method, initially, we assume that B in equation (47) equals to $B_{||}$ in equation (6) at the very radius $r = \lambda_J$ corresponding to the Jeans length, which gives

$$\lambda = \frac{1}{2\pi^2\beta}. \quad (53)$$

With aforementioned formulae, we further adopt an ideal parameter set in which $T \sim 10$ K, $\mu \sim m_{H2}$, $a \sim 0.2 \text{ km} \cdot \text{s}^{-1}$, $n \sim 10^5 \text{ cm}^{-3}$, and $\beta \sim 0.507$. In this case ($\lambda \sim 0.1$), the magnetic field is not so strong but dominating ($\beta < 1$), and it is an reasonable estimation that $B \sim 81 \ \mu$G compared with observational results (e.g. those of NGC 2024, OMCN-4 (Crutcher 1999) or other molecular clouds (Bourke et al. 2001)). Theoretically, parameters from any Class I converging isothermal MHD shock solution with $\lambda = 0.1$ can be used to derive t_0 and r_s. Here we only consider a3[14] and work out its pure hydrodynamical coun-

---

[13] Strictly speaking, according to the self-similar MHD transformation formula $\rho = \alpha/(4\pi Gt^2)$, the core density diverges as $t \to 0_-$, since as $x \to 0_+$, $\alpha \to D$. In fact, when the gas at the core

is dense enough, nuclear reactions would occur, and our highly ideal isothermal MHD model is not applied to the core involving nuclear reactions. However, our model can delineate the evolution of the formation environment of the core in a much larger scale (compared with the core itself), based on the presumption that the feedback of the core (i.e. radiation produced by nuclear reactions) to its environment is negligible in this collapse-triggering process and the isothermal condition is valid.

[14] Other solutions produce unphysical results, e.g. r_ss larger than the size of the molecular cloud. That is why we give up a1 and a2, despite that they may serve as counterparts of the converging HD shock solutions in Lou & Shi (2014). In fact, some calculation mistakes in Section 7.1 of Lou & Shi (2014) caused a wrong choice of solution, i.e. actually, (following its definitions of symbols), $t_0 \approx -7.91 \times 10^5 \text{ yr} \times \sqrt{10} \approx -2.5 \times 10^6 \text{ yr}$, and $r_s \approx 0.16 \text{ pc} \times \sqrt{10} \approx 0.51$ pc, which contradicts its pre-supposition that the molecular cloud has a size 0.2 pc.

Table 5. Results of the Class I converging isothermal MHD shock solution a3 and its ordinary HD counterpart a3' with the same $x_{sd} = 3.5$, both constructed by Type 1 eigensolutions. $\lambda = 0.1$ for a3, while $\lambda = 0$ for a3'. $x_2 = 500.0$ for calculating approximately the values of the velocity and mass parameters V and A. Note that the free-fall time scale $t_{ff} \sim 1.16 \times 10^5$ yr in this case is at the same magnitude with t_0s for both the MHD and HD model, and the r_ss are also comparable, however, smaller than the size of the molecular cloud, the results here are not likely to be completely unphysical. While for solution a1 and a2, the initial spatial scales of the isothermal MHD shock are 0.78pc and 10.06pc, respectively, which tends to be unrealistic.

L	$t_0[10^5\text{yr}]$	D	x_{su}	$m(x_{su})$
a3	1.14	3.6328	6.9058	25.16
a3'	0.77	1.6658	8.8421	52.92

L	$r_s[\text{pc}]$	$M_s[M_\odot]$	$V\tau$	$A\tau^2$
a3	0.16	5.46	8.2476	33.1655
a3'	0.14	7.79	13.0862	86.4787

terparts a3' with the completely same method and the same x_{sd} for comparison (see Figure 21). The results of t_0, r_s and M_s by the same parameter set is listed in Table 5.

It is shown that the dynamic time scale t_0 of the magneto-hydrodynamic (MHD) model is larger than that of the pure hydrodynamic (HD) model, and the spatial scale r_s of the former is also slightly larger than that of the latter, while the enclosed mass of the former is smaller than that of the latter. Besides, $V\tau$ and $A\tau^2$ of the MHD solution are smaller than those of the HD solution by factors 37% and 62%, respectively. In both case, the shock and the outer envelope behind the shock travel supersonically. Therefore, our results agree well with the conclusions of Heitsch et al. (2001) that the weakly magnetized turbulence can reduce the density enhancements behind shocks (as indicated by a smaller $A\tau^2$) and, thus, slow down (as revealed by a smaller $V\tau$ and, perhaps, a larger t_0) and weaken (as seen from a smaller M_s) the process of isolated collapse. This demonstrates that our highly idealized model does portray the supersonic large-scale shock-triggering process for the core collapse of protostar formation in magnetized molecular clouds.

6.2.2 Converging isothermal MHD shocks for supernovae

As mentioned by Lou & Shi (2014), spherical shock wave can be triggered in massive progenitors during implosion process in gravitational collapse by the impact of different gas layers and propagate to the centre with a shrinking shock front and enhancing shock strength, leaving non-linear disturbance behind, which may initiate supernovae explosion. With this picture in mind, our converging isothermal MHD shock solutions serve as illustrating examples for lots of theoretical possibilities of pre-supernovae evolution and supernovae explosion.

For Type Ia supernovae (SNIa) from thermal nuclear explosion, sub-Chandrasekhar mass white dwarfs are possible progenitors with a special explosion mechanism in which converging shocks are involved: If the accretion rate of the He-shell is low enough, the accreted He is accumulated instead of fused to C and O, which can generate violent det-
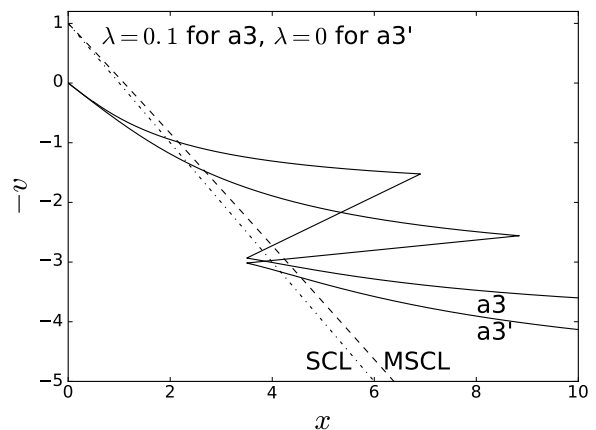

Figure 21. The $-v$ versus x diagram of a3 and a3'. The dashed line is the MSCL for $\lambda = 0.1$ (MSCL), while the dashed dotted line corresponds to the sonic critical line for $\lambda = 0$ (SCL). Given the same x_{sd}, the converging isothermal MHD shock has a smaller $\tau(a3) = 1.9731$ than the ordinary converging isothermal HD shock $\tau(a3') = 2.5263$. After the shock, for the MHD model a3, the velocity and mass parameters of the outer envelope $V = 4.18$ and $A = 8.519$, while for the HD model a3', $V = 5.18$ and $A = 13.55$ (calculated at the approximate infinity $x_2 = 500.0$). Other pertinent parameters are contained in Table 5

onations in the He-shell after reaching a critical amount of He (Fink et al. 2007). The detonation of He creates a converging shock which propagates towards the centre and may trigger the secondary detonation of the C-O core directly or delayed (Fink et al. 2010). The second converging shock emerges while the C-O core is ignited. This scenario seems relevant to our twin converging isothermal MHD shock solutions. Besides, according to Wickramasinghe & Ferrario (2000), 5% of all isolated white dwarfs have magnetic fields ranging from $\sim 3\times10^4$ to $\sim 10^9$G, and 25% of interacting binaries involve magnetic white dwarfs with fields in the range $\sim 10^7 - 10^8$G[15]. Therefore, it is of significance to investigate magnetic fields in SNIa explosions including those from sub-Chandrasekhar mass white dwarfs. Since the core of white dwarfs is supported by degenerate electrons whose evolution is better delineated by conventional or general polytropic process, our twin converging isothermal MHD shock solutions are not suited quantitatively to the 'double-detonation' SNIa of sub-Chandrasekhar mass magnetic white dwarfs. However, grossly speaking, we may expect the similar effects of the magnetic field as those for magnetised molecular clouds, i.e. larger time-scale and spatial scale, weaker density enhancement behind the shock as well as smaller enclosed mass defined by the emergence of the shock. It would be of considerable interest to study converging isothermal MHD shocks in conventional or general polytropic MHD model framework developed by Wang & Lou (2008) and (Lou & Hu 2010) to attain better understandings of the roles played by magnetic fields in SNIa explosions.

---

[15] These statistics might be out of date. The point here is that magnetic white dwarfs are not rare, especially in binary systems where SNIa are created.

As to other types of supernovae (i.e. core-collapse supernovae) whose progenitors are more massive stars, the propagation of a converging shock may also emerge in the pre-explosion phase, and magnetic fields can play even more important roles, especially when rotation is taken into account.

For the presupernovae evolution, it is shown by Akiyama & Wheeler (2004) that even a relative modest initial rotation of the iron core (with a period of $\sim 6 - 31$s) would result in a very rapidly rotating protoneutron star and exponential growth of the magnetic field by the magnetorotational instability (MRI) (even to an order $10^{15} - 10^{16}$G), which can power MHD bi-polar flow or jets related to the asymmetry of the core-collapse supernovae. Heger et al. (2005) investigated the presupernovae evolution of differentially rotating massive stars including magnetic fields under consideration of magnetic braking, dynamo process in radiative, semiconvective and thermohaline regions, indicating that the magnetic torque would decrease the final rotation rate of the collapsing iron core. After the core bounce, the new born magnetar with a fast rotation rate and a strong magnetic field is also considered to be a possible power source of Type Ib/c supernovae (Woosley 2010; Inserra et al. 2013) and long duration gamma-ray bursts (GRBs) (Metzger et al. 2011) through dipole emission, magnetic dissipation as well as magnetar winds and shocks, as it spins down and transports out rotational energy.

Our highly ideal spherically symmetric isothermal MHD model does not consider the rotation and may only provide sensible approximations to certain stage of the above scenario. That is to say, at the latest stage of presupernovae evolution, the dynamo effectively stops tracking the changing conditions and the field is frozen in (Heger et al. 2005), as a result, our approximate random traverse magnetic field is applicable. Similar to the last section on magnetised molecular clouds, we use Class I converging isothermal MHD shock solution a1 with $\lambda = 0.1$ to delineate the latest presupernovae evolution stage. Consider a quasi-spherical converging isothermal shock triggered during the latest stage of core collapse by the impact of different gas layers (and, perhaps, driven by MRI), it propagates towards the center, leaving behind compressed turbulent high-speed infall flows. This process is accompanied by the increase of core density and the bounce of the core would occur when the shock front 'reaches' the center (see footnote 13). As an example for illustration, for a typical progenitor with a mass $\sim 15 \ M_\odot$, on the onset of the latest stage, we have the central mass density $\rho_0 = n\mu \sim 8.7 \times 10^9 \ \mathrm{g \cdot cm^{-3}}$ and the assumed uniform temperature $T \sim 6.84 \times 10^9$ K (Heger et al. 2005). Then the sound speed is

$$a = (k_B T/\mu)^{1/2} = 6.51 \times 10^3 \ \mathrm{km \cdot s^{-1}} \ , \qquad (54)$$

where $\mu = 4m_p/3 \approx 2m_{H_2}/3$ is the mean particle mass for a fully ionized helium gas and $m_p = 1.67 \times 10^{-24}$ g is the proton mass. Then by formula (48), we derive the dynamic time scale of this process

$$t_0 = \sqrt{\frac{D}{4\pi G\rho_0}} = 0.689 \ \mathrm{s} \ , \qquad (55)$$

where $D = e^{8.15} \approx 3463$ is the central reduced density parameter for a1. The dynamic scale $t_0 = 0.689$ s here is close to the death time ~ 0.5 s given by Heger et al. (2005) and

slightly larger than it, which can be explained by the same argument in footnote 13 that the shock front never really reaches the centre and the bounce of the core would occur after a time interval shorter than t_0. From formulae (49) and (50), the spatial scale of the shock r_s and the enclosed mass defined by the emergence of the shock M_s are

$$r_s = ax_{su}t_0 = 4.84 \times 10^8 \ \mathrm{cm} \ , \qquad (56)$$

$$M_s = \frac{a^3 t_0}{G} m(x_{su}) \sim 2.97 \ M_\odot \ , \qquad (57)$$

where $x_{su} = x_s = 1.08$, $m(x_{su}) = 2.0732$ for a1. Interestingly, r_s and M_s are also of the same order with $R_{smap} = 1.2 \times 10^8$ cm and $M_{samp} = 1.3 \ M_\odot$ from Heger et al. (2005), respectively.

Just before the bounce of the core, the shock front is very close to the centre and we can use the large-x asymptotic solution (16) and (17) to specify the infall flow speed as well as the density profile after the shock (i.e. the outer region other than the core), following formulae (51) and (52):

$$u \sim -aV\tau = 3.31 \times 10^3 \ \mathrm{km \cdot s^{-1}} \ , \qquad (58)$$

$$\rho \sim \frac{a^2}{4\pi G r^2} A\tau^2 = 1.34 \times 10^8 \ \mathrm{g \cdot cm^{-3}} \left(\frac{r}{10^8 \ \mathrm{cm}}\right)^{-2} \ , \quad (59)$$

where $\tau = 1$ (one-temperature isothermal MHD converging shock), and the velocity and mass parameters for a1 $V = 0.509$, $A = 2.651$ (see Table 2). The infall flow speed exceeds the criterion infall speed $10^3 \ \mathrm{km \cdot s^{-1}}$ for the latest presupernovae phase of Heger et al. (2005), and the density at $r = R_{samp} = 1.2 \times 10^8$ cm is $\sim 9.3 \times 10^7 \ \mathrm{g \cdot cm^{-3}}$ which is also of the same order with $\rho_{samp} = 5 \times 10^7 \ \mathrm{g \cdot cm^{-3}}$ given by Heger et al. (2005). Finally, the magnetic field strength and the parameter $\beta = p_{th}/p_m$ can be estimated by the combination of the frozen in condition (5) and the density profile formula (52), given $A = 2.651$, $\tau = 1$ and $\lambda = 0.1$, as

$$B \sim \frac{a^2}{r\sqrt{G}} A\tau^2\sqrt{\lambda} = 1.375 \times 10^{15} \ \mathrm{G} \left(\frac{r}{10^6 \ \mathrm{cm}}\right)^{-1} \ , \qquad (60)$$

$$\beta = \frac{8\pi\rho a^2}{B^2} \sim \frac{2}{A\tau^2\lambda} = 7.54 \ . \qquad (61)$$

It is shown that for the typical radius of a neutron star $r \sim 10^6$ cm, the magnetic field has a strength $\sim 1.375 \times 10^{15}$ G of the same order with the prediction of MRI (see Figure 3 of Akiyama & Wheeler (2004)), and the parameter $\beta^{-1} = 13.3\%$ also agrees well with that (above 10%) from MRI (Akiyama & Wheeler 2004).

The above analysis of a1 demonstrates that, despite the simpleness of our quasi-analytical model for an ideal non-rotating isothermal magnetofluid, the agreement with results from more complicated simulations with rotation is surprisingly good. Besides, it is possible to construct a sequence of converging MHD shock solutions under different values of λ to produce different τ, V and A values. However, the quasi-spherical symmetry, the random traverse magnetic field and the isothermal condition are great simplifications to the real physical process of presupernovae evolution, the agreement above merely implies that turbulence (instabilities) and shock waves in the context of MHD (which are the features shared by our model and other more complicated models) are of great importance to understand core-collapse supernovae , and our non-linear converging isothermal MHD shock solutions may provide important benchmarks for testing numerical codes for MHD under self-gravity.

Beyond the presupernovae phase, we can also imagine the explosion itself with the converging isothermal MHD shock solution by connecting it with the void expansion solution with outgoing isothermal MHD shocks in the old solution space (see Section 2.2 for the relations between the new solution space and the old solution space) to describe a MHD converging-shock-rebound-void-expansion-shock (CSRVES) process. Consider a converging isothermal MHD shock for a MHD LP-type solution approaching the centre as $t \to 0-$, the density $\rho \propto \alpha/t^2 \to D/t^2$ at the centre is divergent, which is beyond the range of our simplified model, therefore, the isothermal MHD shock never really reaches the centre. It is supposed that other more complicated physical processes (e.g. nuclear burning, radiation pressure, degenerate materials, electrons and neutrinos) will be involved in a small central region which finally generate a rebounded outgoing isothermal MHD shock which breaks out of the stellar surface in the time scale t_{break} and is followed by an expanding void. We assume that the spherical symmetry holds in this scenario. Similar to the theoretical model for wind-wind dynamic interaction for X-ray emissions from PNe where isothermal gas dynamics of central voids and surrounding envelopes with or without shocks are studied (Lou & Zhai 2009), the after-rebound effective void here can be regarded as an inner wind zone in which wind heated by neutrinos expands freely from the surface of the protomagnetar into the cavity generated by the precedent rebound shock launched by neutrino heating or MHD forces (Metzger et al. 2011). We assume that whatever the rebound mechanism is, at the very instant when the rebound occurs, it mainly changes the velocity of the flow on the boundary of the small central region (which grossly becomes the void later), while the density ρ_b of the fluid on the boundary as well as the properties of the outer envelope remain almost unchanged. Therefore, when constructing the after-rebound branch of any CSRVES solution in the old solution space (i.e. $\widetilde{x}$ and $\widetilde{v}$), we require that the dimensionless density $\widetilde{\alpha}_0$ on the boundary of the expanding MHD void equals to the central reduced density parameter D of the MHD LP-type solution from the before-rebound branch to specify that $\rho_b^{before} \sim \rho_b^{after}$ (i.e. grossly speaking, $D = \lim_{t \to 0_-} \alpha \sim \lim_{t \to 0_+}^{r=\widetilde{x}_1 ta} \widetilde{\alpha} = \widetilde{\alpha}_0$) and that the parameters of the outer envelope satisfy the relations that $-V = \widetilde{V}$ and $A = \widetilde{A}$.

As an example, following the above analysis of presupernovae evolution with $\lambda = 0.1$, we again use a1 (see Table 2) as the before-rebound branch (i.e. $t : -t_0 \to 0_-$, $x : r/(at_0) \to +\infty$ for any fixed r), so that $\alpha_0 = D = e^{8.15} \approx 3463$, $\widetilde{V} = -V = -0.509$, and $\widetilde{A} = A = 2.651$. Then we construct the after-rebound branch (i.e. $t : 0_+ \to t_{break}$, $\widetilde{x} : +\infty \to r/(a\tau_0 t_{break})$[16] for any fixed r) by applying the standard $\widetilde{\alpha}$ versus $\widetilde{v}$ phase diagram matching method to outward integrations from varying starting point $\widetilde{x}_1$ (with fixed $\widetilde{\alpha}_0$) and inward integrations from $\widetilde{x}_2 = 500.0$ (with constant $\widetilde{V}$, and $\widetilde{A}$) shocked at $\widetilde{x}_{su}$s by fixed $\widetilde{x}_{sd} = 1.05$

and different values of $\tau = \widetilde{x}_{su}/\widetilde{x}_{sd}$ under Type 2 two-temperature isothermal MHD shock condition to a given meeting point $\widetilde{x}_m = 0.8$, as shown in Figure 22, which specifies that $\widetilde{x}_1 = 0.03195$, $\tau = 1.4903$, and $\widetilde{x}_{su} = 1.5648$. The results of the fluid velocity $-v = \widetilde{v}$, the radio of the Alfvén speed to the sound speed v_A/a, the density parameter $\alpha = \widetilde{\alpha}$ and the magnetic field parameter $b = \widetilde{b}$ as functions of x or $\widetilde{x}$ are displayed in Figure 23 and 24. With these results, and the same set of parameters for the presupernovae evolution, we can speculate the expansion rate of the central void u_v as well as the velocity u_s of the outgoing isothermal MHD shock shortly after the rebound (i.e. the temperature does not drop too much):

$$u_v = a\widetilde{x}_1 \sim 208 \text{ km} \cdot \text{s}^{-1} \ , \tag{62}$$

$$u_s = a\widetilde{x}_{su} \sim 1.02 \times 10^4 \text{ km} \cdot \text{s}^{-1} \ . \tag{63}$$

where the sound speed a is approximately unchanged after the rebound given by formula (54). Given the typical radius of such a 15 $M_\odot$ progenitor $R_s \sim 10^{12}$ cm, the time scale for the outgoing shock to break out of the stellar surface is $t_{break} \sim R_s/u_s \sim 10^3$ s.

An important feature of this scenario is that properties of the after-rebound branch isothermal MHD void expansion solution (i.e. the void boundary $\widetilde{x}_1$, the shock strength parameter τ) are completely determined by the before-rebound branch LP-type MHD solutions involving a converging isothermal MHD shock and the downstream shock position $\widetilde{x}_{sd}$. In our highly simplified isothermal model, it is difficult to use other asymptotic MHD solutions as the after-rebound branch, so the MHD void expansion solution is the best choice, however, does not provide any information of the new born central magetar. Therefore, future study may focus on the converging shocks in the conventional or general polytropic MHD model (Wang & Lou 2008; Lou & Hu 2010), where more asymptotic solutions, e.g. the MHD counterpart of the new quasi-static solution with divergent mass density approaching the core and self-similar oscillations (Lou & Wang 2006), can be found to delineate magnetars created in supernovae explosions.

6.2.3 Contracting voids with converging isothermal MHD shocks

In broad contexts of astrophysics (e.g. H_{II} regions formed around protostars, planetary nebulae, core collapse supernovae explosions and remnants), a central void (or cavity/bubble) of relatively low density may occur in contact with the massive outer envelope, when the central region provides sufficient pressure against the gravity to push outward materials at certain stage of evolution, during which process shocks may be involved. Later on the void may experience expansion or collapse regarding variances of the central pressure source and the environment.

During the past few years, in the framework of self-similar hydrodynamics and magetohydrodynamics for isothermal, conventional polytropic (CP) and general polytropic (GP) gas under self-gravity, since the zero mass line (i.e. $m(x_1) = 0$, where m is the enclosed mass parameter and x_1 is the very value of the self-similar independent variable x relevant to evolution of the void boundary) is a general structure in the solution space, self-similar solutions (with

---

[16] In fact, after the rebound, the sound speed shifts from a to $\tau_0 a$, where τ_0 is the shock strength parameter of the before-rebound MHD shock solution. In our case, the shock of the before-rebound branch is an one-temperature isothermal converging MHD shock with $\tau_0 = 1$, and, thus, the speed of sound remains unchanged.
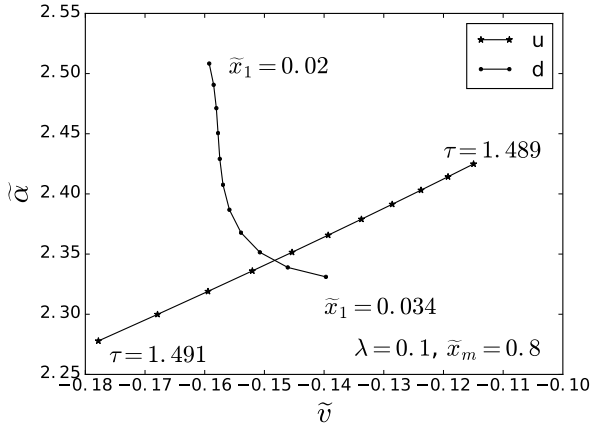
Figure 22. Examples of the $\widetilde{\alpha}$ versus $\widetilde{v}$ loci in search of the after-rebound MHD void-expansion-shock solution with $\lambda = 0.1$ and $\widetilde{x}_m = 0.8$ in the old solution space. The upstream locus (marked by asterisks, labelled by 'u') is formed by inward integrations starting from the large-$\widetilde{x}$ asymptotic MHD solution with the velocity and mass parameters $\widetilde{V} = -V = -0.509$, and $\widetilde{A} = A = 2.651$ at the approximated infinity $\widetilde{x}_2 = 500.0$, involving shocks at $\widetilde{x}_{sd} = 1.05$ with different values of τ in the range of $1.486 \sim 1.488$. The downstream locus (marked by solid dot, labelled by 'd') is produced by outward integrations with different starting points $\widetilde{x}_1$s on the void boundary in the range of $0.02 \sim 0.034$, given fixed dimensionless density $\alpha_0 = D = e^{8.15}$. The final result of a series of such diagrams is that $\widetilde{x}_1 = 0.03195$, and $\tau = 1.4903$.
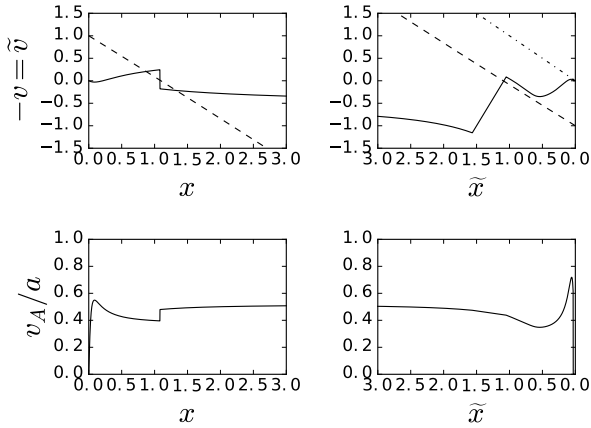
Figure 24. The a versus x diagram (upper left), $\widetilde{a}$ versus $\widetilde{x}$ diagram (upper right), b versus x diagram (lower left) and $\widetilde{b}$ versus $\widetilde{x}$ diagram (lower right) of the exemplar CSRVES solution with $\lambda = 0.1$. α, $\widetilde{\alpha}$, b and $\widetilde{b}$ axes are all in the logarithmic scale. The dashed line is the MSCL.

Figure 23. The $-v$ versus x diagram (upper left), $\widetilde{v}$ versus $\widetilde{x}$ diagram (upper right), v_A/a versus x diagram (lower left) and v_A/a versus $\widetilde{x}$ diagram (lower right) of the exemplar CSRVES solution with $\lambda = 0.1$. The dashed line is the MSCL, while the dashed dotted line corresponds to the ZML $\widetilde{x} = \widetilde{v}$. The left two diagrams of the before-rebound branch belong to the new solution space with $t < 0$, while the right two of the after-bound the old with $t > 0$. The two branches of are connected at $x \to +\infty$ and $\widetilde{x} \to +\infty$ as $t \to 0_-$ and $t \to 0_+$ by the consistency that $-V = \widetilde{V} = -0.509$ and $A = \widetilde{A} = 2.651$.

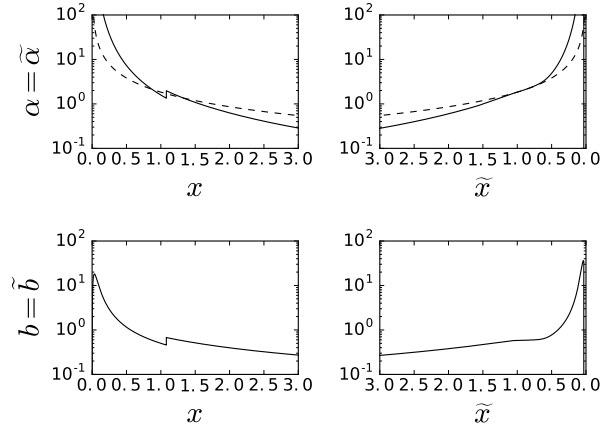or without shocks) of voids connected to surrounding dense envelopes with inflows or outflows have been constructed for various astrophysical applications and compared with simulation and observation results (Hu & Lou 2008; Lou & Cao 2008; Lou & Wang 2012; Lou & Hu 2010; Lou & Zhai 2009).

For instance, as described by the self-similar 'champagne flow' shock solution for polytropic gas from Hu & Lou (2008), after the inner part of a certain cloud has fallen into a new-born protostar, a central expanding voids can be carved out by powerful stellar wind, and associated with outgoing shocks generated by intense and rapid UV photoionization of ambient medium surrounding the burning protostar. Besides, during the core collapse of a supernova progenitor, as central density becomes sufficiently high, neutrinos of relativistic energies are released when formation of neutrons occurs in the core. Since the neutrino opacity is extremely high in such an environment of high-density, the resulting neutrino pressure may become overwhelming and, together with radiation pressure and gas pressure, push the outer part to expand, in which process a central void starts to form (Lou & Cao 2008). As the expansion lowers down the density, neutrinos escape during the decoupling, the left radiation field and plasma pressure may continue drive the expansion of the void (Lou & Wang 2012). This scenario were portrayed by self-similar void solutions for a relativistic gas (regrading neutrinos with negligible mass and photos in the high-density core) of (general) polytropic index $\gamma = 4/3$ (Lou & Cao 2008), for a CP gas (Lou & Wang 2012) and for a GP magnetofluid (Lou & Hu 2010). Moreover, for a planetary nebulae as the late phase of stellar evolution, the inner hot, fast, tenuous stellar wind involving a reverse shock forms a wind zone which can be regarded as an effective void expanding after a forward shock running into the massive outer AGB (slow) wind envelope. This process is shown properly described by self-similar isothermal void expansion solutions with outgoing shocks (Lou & Zhai 2009). Such solutions can also be applied to a similar scenario in a larger scale for evolution of interstellar medium

(ISM, e.g. H_{II} region) around early-type stars or Wolf-Rayet stars whose wind zones also serve as effective voids.

The aforementioned theoretical models show the powerfulness of self-similar approach for delineating voids, however only consider expanding voids. Actually, in the same astrophysical backgrounds, collapse or contraction of voids may also occur (Lou & Shi 2014) : For core collapse supernovae, when central neutrinos and radiation leak out through the outer envelope as density drops sufficiently, the pressure can be overwhelmed by gravity, resulting in central void contraction. For wind-supported voids in PH and ISM, when the central wind becomes weaker gradually, voids would start to shrink. Along with the central void contraction, converging shocks can also occur due to impacts among different layers of gas in the outer envelope. In the present work, through a time-reversal operation, we construct several self-similar isothermal MHD solutions whose centres are shrinking voids without (see Table 1 and Figure 2) and with (see Table 3 and Figure 11-13) isothermal MHD converging shocks, which can be regarded as an extension of the previous work by Lou & Zhai (2009) that investigated the isothermal gas dynamics of central voids and surrounding envelopes with or without shocks systematically. And our model is more realistic in consideration of a random traverse magnetic field. Here we focus on the effect of magnetic fields on construction of such self-similar isothermal (converging) void solutions. For comparison, we construct the HD counter parts of self-similar isothermal MHD void solutions v1-v4 as v1'-v4', which start from the same x_1s and cross the SCL smoothly at x'_*s as Type 1 eigensolutions. The results of x_* and the dimensionless density at the void boundary α_0 of both MHD and HD models are shown in Table 6.

We find that at the same void boundary x_1, the value of α_0 are smaller in the HD model than that in the MHD model with $\lambda = 0.1$. Besides, for both HD and MHD models, the value of α_0 decreases as x_1 increases. So we may further infer that given the same value of α_0, the corresponding x_1 in the MHD model would be larger than that in HD model. As for x_*, there is no consistent difference between results of the two models at different x_1s. As illustrated by the self-similar transformation formulae (7), given certain temperature (i.e. speed of sound), x_1 is proportional to the speed of the boundary between the central void and the massive outer envelope (i.e. the void contacting or expanding rate), while α_0 is proportional to the density difference (i.e. discontinuity) at the boundary (, since the density inside the void is negligible). So we conclude that the for the same void contracting or expanding rate, the density discontinuity at the edge of the central void for a magnetized gas is more significant than that for an ordinary gas without magnetic fields, while for the same density discontinuity, the void would contract or expand faster in a magnetofluid than in an ordinary fluid.

ACKNOWLEDGEMENTS

Table 6. The results of x_* and the dimensionless density at the void boundary α_0 of self-similar isothermal void solutions in the MHD model with $\lambda = 0.1$ and those in the HD model with $\lambda = 0$, in which the void boundaries x_1s are the same for the two models. It is shown that at the same void boundary x_1, the value of α_0 are smaller in the HD model than that in the MHD model with $\lambda = 0$. As to x_*, there is no consistent difference between results of the two models at different x_1s.

$\lambda = 0.1$	v1	v2	v3	v4
x_1	0.85	0.4	0.04	0.004
α_0	1.8004	2.8406	3.6487	3401
x_*	2.5013	2.2313	2.1641	0.8705
$\lambda = 0$	v1'	v2'	v3'	v4'
x_1	0.85	0.4	0.04	0.004
α_0	1.3216	1.5741	1.6649	1708
x_*	2.4990	2.3610	2.3411	0.7388

REFERENCES

Akiyama S., Wheeler J. C., 2004, in , Stellar Collapse. Springer, pp 259–275
Bian F.-Y., Lou Y.-Q., 2005, MNRAS, 363, 1315
Bourke T. L., Myers P. C., Robinson G., Hyland A., 2001, ApJ, 554, 916
Chevalier R. A., 1997, ApJ, 488, 263
Courant R., Friedrichs K. O., 1976, Supersonic Flow and Shock Waves. Springer-Verlag, New York
Crutcher R. M., 1999, ApJ, 520, 706
Fink M., Hillebrandt W., Röpke F., 2007, A&A, 476, 1133
Fink M., Röpke F., Hillebrandt W., Seitenzahl I., Sim S., Kromer M., 2010, A&A, 514, A53
Guderley G., 1942, Luftfahrtforschung, 19, 302
Heger A., Woosley S., Spruit H., 2005, ApJ, 626, 350
Heitsch F., Mac Low M.-M., Klessen R. S., 2001, ApJ, 547, 280
Hidalgo J., Mendoza S., 2005, Phy. Fluids (1994-present), 17, 096101
Hu R.-Y., Lou Y.-Q., 2008, MNRAS, 390, 1619
Hunter C., 1977, ApJ, 218, 834
Inserra C., et al., 2013, ApJ, 770, 128
Klessen R. S., 2001, ApJ, 556, 837
Kushnir D., Livne E., Waxman E., 2012, ApJ, 752, 89
Landau L. D., Lifshitz E. M., 1987, Fluid Mechanics. England Pergamon Press, Oxford
Larson R. B., 1969, MNRAS, 145, 271
Lazarus R. B., 1981, SIAM J. Numer. Anal., 18, 316
Lou Y.-Q., Cao Y., 2008, MNRAS, 384, 611
Lou Y.-Q., Gao Y., 2006, MNRAS, 373, 1610
Lou Y.-Q., Hu R.-Y., 2010, New Astron., 15, 198
Lou Y.-Q., Shen Y., 2004, MNRAS, 348, 717
Lou Y.-Q., Shi C.-H., 2014, MNRAS, 442, 741
Lou Y.-Q., Wang W.-G., 2006, MNRAS, 372, 885
Lou Y.-Q., Wang L., 2012, MNRAS, 420, 1897

Lou Y.-Q., Zhai X., 2009, Ap&SS, 323, 17

McKee C. F., Ostriker E. C., 2007, A&A, 45, 565

Metzger B. D., Giannios D., Thompson T. A., Bucciantini N., Quataert E., 2011, MNRAS, 413, 2031

Meyer-ter Vehn J., Schalk C., 1982, Z. Naturforsch. A, 37, 954

Oren Y., Sari R., 2009, Phys. Fluids, 21, 106102

Pan M., Sari R., 2006, ApJ, 643, 416

Penston M., 1969, MNRAS, 144, 425

Shen Y., Lou Y.-Q., 2004, ApJ, 611, L117

Shu F. H., 1977, ApJ, 214, 488

Shu F. H., Lizano S., Galli D., Cantó J., Laughlin G., 2002, ApJ, 580, 969

Tsai J. C., Hsu J. J., 1995, ApJ, 448, 774

Wang W.-G., Lou Y.-Q., 2008, Ap&SS, 315, 135

Whitworth A., Summers D., 1985, MNRAS, 214, 1

Wickramasinghe D., Ferrario L., 2000, PASP, 112, 873

Woosley S. E., 2010, ApJ, 719, L204

Yu C., Lou Y.-Q., 2005, MNRAS, 364, 1168

Yu C., Lou Y.-Q., Bian F.-Y., Wu Y., 2006, MNRAS, 370, 121

APPENDIX A: THE IDEAL MHD APPROXIMATION

The magnetic induction equation is

$$\frac{\partial \mathbf{B}}{\partial t} = \nabla \times (\mathbf{u} \times \mathbf{B}) + \frac{1}{4\pi\sigma}\nabla^2 \mathbf{B} \ , \tag{A1}$$

where σ is the electrical conductivity which is assumed to be infinite. Then we note down the following equations as three component forms:

$$\frac{\partial B_r}{\partial t} = \frac{1}{r\sin\theta}\frac{\partial}{\partial \theta}\left[\sin\theta\left(u_r B_\theta - u_\theta B_r\right)\right]$$
$$-\frac{1}{r\sin\theta}\frac{\partial}{\partial \phi}\left(u_\phi B_r - u_r B_\phi\right) \ , \tag{A2}$$

$$\frac{\partial B_\theta}{\partial t} = \frac{1}{r\sin\theta}\frac{\partial}{\partial \phi}\left(u_\theta B_\phi - u_\phi B_\theta\right) - \frac{1}{r}\frac{\partial}{\partial r}\left[r\left(u_r B_\theta - u_\theta B_r\right)\right] \ , \tag{A3}$$

$$\frac{\partial B_\phi}{\partial t} = \frac{1}{r}\frac{\partial}{\partial r}\left[r\left(u_\phi B_r - u_r B_\phi\right)\right] - \frac{1}{r}\frac{\partial}{\partial \theta}\left(u_\theta B_\phi - u_\phi B_\theta\right) \ , \tag{A4}$$

where $u_r = u$ and $u_\phi \cong 0$, $u_\theta \cong 0$ by the presumed quasi-spherical symmetry. PDE (A2) takes the form

$$\frac{\partial B_r}{\partial t} = u_r\left(\nabla_{||}\cdot\mathbf{B}_{||}\right) + \left(\mathbf{B}_{||}\cdot\nabla\right)u_r \ , \tag{A5}$$

where $\nabla_{||} = (1/r)\,\partial_\theta\widehat{\theta} + [1/\left(r\sin\theta\right)]\,\partial_\phi\widehat{\phi}$. This PDE can be combined with the divergence free condition $\nabla\cdot\mathbf{B} = 0$ and multiplied with a factor of $r^4 B_r$ on both sides to give

$$\frac{1}{2}\frac{D}{Dt}\left[\left(r^2 B_r\right)^2\right] = r^4 B_r\left(\mathbf{B}_{||}\cdot\nabla\right)u_r \ , \tag{A6}$$

where $D/Dt = \partial_t + u_r\partial_r$. PDEs (A3) and (A4) can be multiplied with $1/B_\theta$ and $1/B_\phi$ respectively, which ends up with

$$\frac{D}{Dt}\ln\left(\frac{B_\theta}{r}\right) = -\frac{1}{r^2}\frac{\partial}{\partial r}\left(r^2 u_r\right) \ , \tag{A7}$$

$$\frac{D}{Dt}\ln\left(\frac{B_\phi}{r}\right) = -\frac{1}{r^2}\frac{\partial}{\partial r}\left(r^2 u_r\right) \ . \tag{A8}$$

Since the equation for mass conservation, i.e. PDE (1) can be written in a similar form

$$\frac{D}{Dt}\ln\rho = -\frac{1}{r^2}\frac{\partial}{\partial r}\left(r^2 u_r\right) \ , \tag{A9}$$

we can conclude from PDEs (A7)-(A9) that

$$\frac{B_\theta}{r\rho} = const. \ , \quad \frac{B_\phi}{r\rho} = const. \ , \quad \frac{B_{||}}{r\rho} = const. \ , \tag{A10}$$

which is exactly the frozen-in condition for the magnetic flux and relates the random transverse magnetic field with the mass density ρ (Yu & Lou 2005).

APPENDIX B: EQUATIONS FOR CALCULATING EIGENSOLUTIONS ACROSS THE MSCL

Equation (30) is obtained by the L'Hospital rule from equation (12) in the form of

$$\left(\frac{\partial F_x}{\partial x} + \frac{\partial F_x}{\partial v}v' + \frac{\partial F_x}{\partial \alpha}\alpha'\right)v' = \frac{\partial F_v}{\partial x} + \frac{\partial F_v}{\partial v}v' + \frac{\partial F_v}{\partial \alpha}\alpha' \ . \tag{B1}$$

Using the following six equations

$$\frac{\partial F_x}{\partial x} = 2(x - v) - 2x\lambda\alpha \ , \tag{B2}$$

$$\frac{\partial F_x}{\partial v} = -2(x - v) \ , \tag{B3}$$

$$\frac{\partial F_x}{\partial \alpha} = -\lambda x^2 \ , \tag{B4}$$

$$\frac{\partial F_v}{\partial x} = (x - v)\left[2\alpha + \frac{2}{x^2}\right] - \frac{2}{x} \ , \tag{B5}$$

$$\frac{\partial F_v}{\partial v} = -2(x - v)\alpha + \frac{2}{x} \ , \tag{B6}$$

$$\frac{\partial F_v}{\partial \alpha} = (x - v)^2 \ , \tag{B7}$$

together with two PDEs (10) and (14) to eliminate α and α' in ODE (B1), we then obtain equation (30).

As for equation (31), it is derived by combination of two ODEs (10) and (14) to α.

APPENDIX C: ANALYSIS OF ISOTHERMAL MHD SHOCK CONDITIONS

With the definitions that $\beta_1 \equiv 8\pi p_1/(B_1^2)$ and $M_1 \equiv u_1/a_1$ at hand, and a substitution of expressions (37) into equation (33), we readily derive

$$Xp_1 + X^2 p_1/\beta_1 + p_1 M_1^2/X = p_1 + p_1/\beta_1 + p_1 M_1^2 \ , \tag{C1}$$

which, after removing the common factor p_1, becomes

$$(X - 1) + (X - 1)(X + 1)/\beta_1 = M_1^2(X - 1)/X \ . \tag{C2}$$

Here, $X = 1$ would be a trivial solution. Then by removing the common factor $X - 1 \neq 0$, algebraic equation (C2) gives

$$1 + (X + 1)/\beta_1 = M_1^2/X \ , \tag{C3}$$

which is equivalent to equation (38) in the main text.

Similarly, equation (44) for two-temperature isothermal MHD shock conditions can be obtained by substituting formulae (43) into equation (42). The original form appears as

$$X^2 a_i^2/\beta_1 + \tau^2 X a_i^2 + M_1^2 a_i^2/X = a_i^2/\beta_1 + a_i^2 + a_i^2 M_1^2 \ . \tag{C4}$$

It is known that $f_{II}(X \to +\infty) \to +\infty$, $f_{II}(X \to -\infty) \to -\infty$, and $f_{II}(X = 0) = \beta_1 M_1^2 > 0$, the cubic equation (44) has at least one negative (real) root of X.

When $\tau < 1$, $f_{II}(X = 1) = \beta_1 (\tau^2 - 1) < 0$. Apparently, equation (44) has three real roots of which one is positive and smaller than 1, while the other positve one is greater than 1.

When $\tau > 1$, $f_{II}(X = 1) > 0$, further analysis is needed to draw meaningful conclusions. We take differentiation of $f_{II}(X)$ with respect to X as $f'_{II}(X) = df_{II}/dX$:

$$f'_{II}(X) = 3X^2 + 2\beta_1 \tau^2 X - \left(1 + \beta_1 + \beta_1 M_1^2\right) , \qquad (C5)$$

from which we can easily find two roots for $f'_{II}(X) = 0$:

$$X_{\pm} = \{-\beta_1 \tau^2 \pm \left[\beta_1^2 \tau^4 + 3\left(1 + \beta_1 + \beta_1 M_1^2\right)\right]^{1/2}\}/3 . \quad (C6)$$

For $f_{II}(X_+) > 0$, there is no real root for $f_{II}(X) = 0$ other than the aforementioned negative root. For $f_{II}(X_+ \le 0)$, there are two positive real roots to make $f_{II}(X) = 0$ (including the repeated root). In the latter case, the two positive roots are either both larger than 1 or both smaller than 1 beacuse $f_{II}(X = 1) > 0$. From above analysis, we arrive at the conclusion in Section 3.2 that the cubic equation (44) may have two positive roots both larger than 1, or have no real root larger than 1.

APPENDIX D: COMPARISON TO THE MHD SHOCK CONDITIONS IN A GENERAL POLYTROPIC MAGNETO-FLUID

This section shows how the equations for MHD shock conditions reduce from their general forms in a (sphericall symmetric) general polytropic magneto-fluid (under self-gravity) of Wang & Lou (2008) to those in an isothermal magneto-fluid of the present paper when $\gamma \to 1$.

The self-similar transformation in Wang & Lou (2008) (formulae (7)) is

$$r = k^{\frac{1}{2}} t^n x , \quad u = k^{\frac{1}{2}} t^{n-1} v , \quad \rho = \frac{\alpha}{4\pi G t^2} ,$$
$$p = \frac{k t^{2n-4}}{4\pi G} \beta , \quad M = \frac{k^{\frac{3}{4}} t^{3n-2} m}{(3n-2)G} , \quad \langle B_t^2 \rangle = \frac{k t^{2n-4}}{G} \omega ,$$
$$(D1)$$

where the definitions of u, ρ, p and M are the same with our work and the B_t here is just the $B_\parallel$ in equation (3).

We further know from the MHD PDEs/ODEs that (equations (11) and (12) in Wang & Lou (2008))

$$\omega = h\alpha^2 x^2 , \quad \beta = \alpha^\gamma m^q , \qquad (D2)$$

where γ is the polytropic index and $q = 2(n + \gamma - 2)/(3n - 2)$. For the polytropic MHD model in Wang & Lou (2008), the effective entropy is conserved, if meanwhile the gas is isothermal, i.e. $p = a^2 \rho$, to reduce to our isothermal model, we must have $n = 1$, $k = A^2 = \gamma a^2$, $h = \lambda$, $\omega = b$, and $\alpha^\gamma m^q = \alpha/\gamma$, which means that $\gamma \to 1$ and $q = 0$, where A is the adiabatic sound speed, a is the isothermal sound speed and λ is the dimensionless parameter that characterises the strength of the magnetic field in our isothermal MHD model defined in formula (6).

The shock conditions expressed by physical quantities

are (expressions (17)-(20) in Wang & Lou (2008)[17])

$$[\rho(u_s - u)]_1^2 = 0 , \qquad (D3)$$

$$\left[p + \rho(u_s - u)^2 + \frac{\langle B_t^2 \rangle}{8\pi}\right]_1^2 = 0 , \qquad (D4)$$

$$\left[(u_s - u)^2 \langle B_t^2 \rangle\right]_1^2 = 0 , \qquad (D5)$$

$$\left[\frac{\rho(u_s - u)^3}{2} + \frac{\gamma p(u_s - u)}{\gamma - 1} + \frac{\langle B_t^2 \rangle}{4\pi}(u_s - u)\right]_1^2 = 0 , \quad (D6)$$

of which equations (D3)-(D5) are equivalent to equations (32)-(34), and euqation (D6) equivalent to equation (35) for (dynamical) MHD energy conservation (which is not well formulated as $\gamma \to 1$, since the second term $\gamma p(u_s - u)/(\gamma - 1)$ diverges). MHD/HD energy conservation is not considered in the isothermal models of Lou & Shi (2014), Yu et al. (2006) and the present work. The following derivations will show that in the isothermal MHD model with $\gamma \to 1$, MHD energy is conserved (dynamically) only when both sides of the shock have the same temperature.

By formulae (D1) and (D2), from equations (D3)-(D6), we obtain the shock conditions in self-similar variables of the general polytropic MHD model (formulae (64) in Wang & Lou (2008)):

$$\alpha_1 \Gamma_1 = \alpha_2 \Gamma_2 , \qquad (D7)$$

$$\alpha_1^{2-n+\frac{3nq}{2}} x_1^{3q-2} \Gamma_1^q + \alpha_1 \Gamma_1^2 + \frac{h\alpha_1^2}{2} = left(\alpha_2, x_2, \Gamma_2) , \qquad (D8)$$

$$\Gamma_1^2 + \frac{2\gamma}{\gamma - 1} \alpha_1^{1-n+\frac{3nq}{2}} x_1^{3q-2} \Gamma_1^q + 2h\alpha_1 = left(\alpha_2, x_2, \Gamma_2) , \qquad (D9)$$

where $left(\alpha_2, x_2, \Gamma_2)$ denotes the formula on the left side of the equal sign with α_1, x_1 and Γ_1 replaced by α_2, x_2 and Γ_2, $\Gamma_i = n - v_i/x_i$, and $\tau = \sqrt{k_2/k_1} = x_1/x_2$, since $u_s = dr_s/dt = nk_i^{1/2} t^{n-1} x_i$ ($i = 1, 2$). And it is necessay to point out that equations (D7)-(D9) correspond to equations (D3), (D4) and (D6), respectively, while equation (D5) has been combined with equation (D3) to give $h_1 = h_2 = h$. We can further eliminate α_2 in equations (D8) and (D9) by equation (D7) to give (equations (65) in Wang & Lou (2008))

$$\alpha_1^{2-n+\frac{3nq}{2}} x_1^{3q-2} \Gamma_1^q + \alpha_1 \Gamma_1^2 + \frac{h\alpha_1^2}{2}$$
$$= \frac{(\alpha_1 \Gamma_1)^{2-n+\frac{3nq}{2}}}{\Gamma_2^{2-n+\frac{(3n-2)q}{2}}} x_2^{3q-2} + \alpha_1 \Gamma_1 \Gamma_2 + \frac{h\alpha_1^2 \Gamma_1^2}{2\Gamma_2^2} , \qquad (D10)$$

$$\frac{2\gamma}{(\gamma - 1)} \alpha_1^{1-n+\frac{3nq}{2}} x_1^{3q-2} \Gamma_1^q + \Gamma_1^2 + 2h\alpha_1$$
$$= \frac{2\gamma}{(\gamma - 1)} \frac{(\alpha_1 \Gamma_1)^{1-n+\frac{3nq}{2}}}{\Gamma_2^{1-n+\frac{(3n-2)q}{2}}} x_2^{3q-2} + \Gamma_2^2 + 2h\frac{\alpha_1 \Gamma_1}{\Gamma_2} , \qquad (D11)$$

of which equation (D11) can be regarded to embody (dynamical) MHD energy conservation since it is directly related to equation (D6) which, as mentioned above, cannot

---

[17] It here uses a pair of square brackets outside each expression enclosed to denote the difference between the upstream (marked by sub-script '1') and downstream (marked by subscript '2') quantities, as has been done conventionally for shock analyses.

be included in the $\gamma \to 1$ isothermal model in a straight forward manner, while equation (D5) corresponds to momentum conservation.

Now, recall the cubic equation (44) and the quadric equation (38) for the two-temperature and one-temperature isothermal MHD shock conditions

$$X^3 + \tau^2 X^2 \beta_1 - \left(1 + \beta_1 + \beta_1 M_1^2\right) X + M_1^2 \beta_1 = 0 , \quad (D12)$$

$$X^2 + (\beta_1 + 1) X - \beta_1 M_1^2 = 0 , \quad (D13)$$

where (formulae (43))

$$\tau = a_j / a_i = x_{si} / x_{sj} , \ M_1 = v_i - x_{si} , \ \beta_1 = 2 / (\lambda x_{si}^2 \alpha_i) ,$$
$$X = \alpha_j / \alpha_i = (v_i - x_{si}) / [\tau (v_j - x_{sj})] . \quad (D14)$$

Our goal is to find the relations among equations (D10)-(D11) and equations (D12)-(D13). For the relations among the variables of these two groups of equations, when we set $(i, \, j) = (1, \, 2)$[18] in formulae (D14), as $\gamma \to 1$, $n \to 1$, $q \to 0$, $k = a^2$, and $h = \lambda$, it turns out that

$$\beta_1 = \frac{2}{h x_1^2 \alpha_1} , \quad M_1 = -x_1 \Gamma_1 , \quad X = \frac{\Gamma_1}{\Gamma_2} . \quad (D15)$$

Then through simple algebra and equations (D15), the reduced (isothermal) version of equation (D10)

$$\alpha_1 x_1^{-2} + \alpha_1 \Gamma_1^2 + \frac{h \alpha_1^2}{2}$$
$$- \frac{\alpha_1 \Gamma_1}{\Gamma_2} \left(\frac{x_1}{\tau}\right)^{-2} - \alpha_1 \Gamma_1 \Gamma_2 - \frac{h \alpha_1^2 \Gamma_1^2}{2 \Gamma_2^2} = 0 \quad (D16)$$

can be easily put into the form

$$\alpha_1 x_1^{-2} \{ 1 + (x_1 \Gamma_1)^2 + \frac{h \alpha_1 x_1^2}{2}$$
$$- \tau^2 \frac{\Gamma_1}{\Gamma_2} - (x_1 \Gamma_1)^2 \frac{\Gamma_2}{\Gamma_1} - \frac{h \alpha_1 x_1^2}{2} \left(\frac{\Gamma_1}{\Gamma_2}\right)^2 \} = 0 , i.e.$$
$$1 + M_1^2 + \frac{1}{\beta_1} - \tau^2 X - \frac{M_1^2}{X} - \frac{1}{\beta_1} X^2 = 0 , \quad (D17)$$

which is exactly equation (D12) for the two-temperature isothermal MHD shock conditions divided by $-X \beta_1$. Here we do not consider equation (D11) for (dynamical) MHD energy conservation at all. So the conclusion is that for two-temperature isothermal MHD shocks, MHD energy does not conserve (dynamically).

Actually, we can eliminate x_2 in equations (D10) and (D11) to give (see equations (66) and (67) in Wang & Lou (2008))

$$\{ \frac{(\gamma + 1)}{2 \gamma} \Gamma_2^2 - \left(\alpha_1^{1-n+\frac{3nq}{2}} x_1^{3q-2} \Gamma_1^{q-1} + \frac{\gamma - 1}{2 \gamma} \Gamma_1 + \frac{h \alpha_1}{2 \Gamma_1}\right) \Gamma_2$$
$$- \frac{2 - \gamma}{2 \gamma} h \alpha_1 \} (\Gamma_2 - \Gamma_1) = 0 , \quad (D18)$$

which can be reduced to the isothermal version as $\gamma \to 1$, $n \to 1$, and $q \to 0$:

$$\left[\Gamma_2^2 - \left(x_1^{-2} \Gamma_1^{-1} + \frac{h \alpha_1}{2 \Gamma_1}\right) \Gamma_2 - \frac{h \alpha_1}{2}\right] (\Gamma_2 - \Gamma_1) = 0 . \quad (D19)$$

---

[18] To be consistent, we also have $x_{s1} = x_1$ and $x_{s2} = x_2$.

By equations (D15), we can write this equation (D19) as

$$\left[(\Gamma_1 x_1)^2 \left(\frac{\Gamma_2}{\Gamma_1}\right)^2 - \left(1 + \frac{h \alpha_1 x_1^2}{2}\right) \frac{\Gamma_2}{\Gamma_1} - \frac{h \alpha_1 x_1^2}{2}\right]$$
$$\times \left(1 - \frac{\Gamma_1}{\Gamma_2}\right) \Gamma_2 x_1^{-2} = 0 , i.e.$$
$$\left[M_1^2 \frac{1}{X^2} - \left(1 + \frac{1}{\beta_1}\right) \frac{1}{X} - \frac{1}{\beta_1}\right] (1 - X) = 0 , \quad (D20)$$

which is exactly equation (D13) multiplied by a factor $(X - 1) / \left(X^2 \beta_1\right)$, and we can throw away the factor $(1 - X)$, since $X = 1$ gives trivial results. This outcome indicates that if we take into account (dynamical) MHD energy conservation by combining equations (D10) and (D11) to attain equation (D18), the MHD shock condition in the general polytropic model will reduce to the one-temperature shock condition in the isothermal model under $\gamma \to 1$. We finally conclude that equation (D6) for (dynamical) MHD energy conservation in the general polytropic model is consistent with the very restriction that $a_1 = a_2$ (i.e. $(k_B T_u / \mu)^{1/2} = a_u = a_d = (k_B T_d / \mu)^{1/2}$, $T_u = T_d$: both sides of the shock have the same temperature) in the $\gamma \to 1$ isothermal model.

APPENDIX E: CLASS III CONVERGING ISOTHERMAL MHD SHOCK SOLUTIONS

Excluding the MHD EWCS, MHD free-fall collapse solutions can be divided into two groups. MHD solutions in Group 1 do not cross the MSCL, while those in Group 2 cross the MSCL twice. In this section, we investigate converging isothermal MHD Shocks relevant to these two groups of MHD free-fall collapse solutions separately.

E0.1 MHD solutions crossing the MSCL once

We connect central MHD free-fall collapse solutions of Group 1 with outer envelopes by taking backward integrations (as Type 1 eigensolutions) from various x_*s to near the origin $x_0 = 10^{-10}$ (at which we infer the approximate central accretion rate $m_0 \approx m(x_0)$ as demonstrated by the leading terms in the small-x asymptotic solution (19)-(20)) involving isothermal MHD shocks at certain x_{sd} with parameters of the downstream and the ordinary two-temperature isothermal MHD shock condition. Five such MHD solutions are shown in Figure E1 and E2. The parameters of these MHD shock solutions are contained in Table E1.

We also construct three converging isothermal MHD shock solutions with the upstream parameters from the EWCS (whose $m_0 \sim 1.0328$), i.e. the magnetostatic outer envelope, as shown in Table E2 and Figure E3.

E0.2 MHD solutions crossing the MSCL more than once

Three converging isothermal MHD Shocks are constructed with three Group 2 MHD free-fall collapse solutions crossing the MSCL at $x_*(1)$ and $x_*(2)$ (Yu & Lou 2005), respectively. Chosen x_{sd}, outward integrations (as Type 1 eigensolutions) from $x_*(2)$ to certain meeting point x_m which experiences shocks at x_{su} under Type 2 two-temperature

Table E1. Five Class III converging isothermal MHD shock solutions constructed by Group 1 MHD free-fall collapse solutions with $\lambda = 0.1$, where $x_2 = 500.0$ for calculating approximately the values of the velocity and mass parameters V and A.

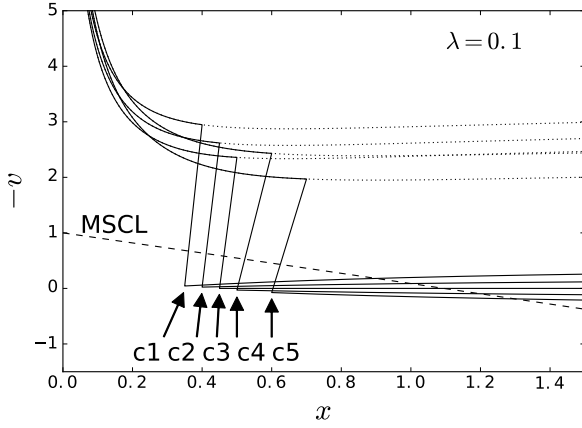| x_{sd}	x_{su}	x_*	V	A	m_0	L
0.35	0.4	0.9	-0.472	1.491	1.0945	c1
0.4	0.45	1.0	-0.225	1.746	1.0804	c2
0.45	0.5	$\sqrt{1.2}$	0	2.0	1.0656	c3
0.5	0.6	1.2	0.235	2.288	1.3586	c4
0.6	0.7	1.3	0.449	2.569	1.3352	c5

Figure E1. The $-v$ versus x diagram of Class III converging isothermal MHD Shocks relevant to Group 1 MHD free-fall collapse solutions with $\lambda = 0.1$. The parameters of the pertinent inner MHD free-fall collapse solutions and the outer envelopes involving shocks are contained in Table E1. The dotted lines are non-shock MHD free-fall collapse solutions with the velocity and mass parameters V_0 and A_0 at the approximate infinity $x_2 = 500.0$ (the curve/MHD solution label L, V_0, A_0): (c1, -3.46, 0.3404), (c2, -3.18, 0.3695), (c3, -2.95, 0.3961), (c4, -2.85, 0.5071), (c5, -2.40, 0.5950). The dashed line is the MSCL.

Table E2. Three Class III converging isothermal MHD shock solutions constructed by the EWSC with $\lambda = 0.1$, where $x_2 = 500.0$ for calculating approximately the values of the velocity and mass parameters V and A. We use Type 1 eigensolutions starting from the MSCL both at $\sqrt{1 + 2\lambda}$ (to integrate outwards as the magnetostatic envelope of EWCS involving shocks at x_{su} to x_m) and x_* (to integrate backwards to x_m).

x_{sd}	x_{su}	x_*	τ	V	A	L
1.6	1.7313	1.9724	1.0821	1.63	4.415	s1
1.7	1.8945	2.1478	1.1144	1.87	4.833	s2
1.8	2.0753	2.3297	1.1529	2.10	5.233	s3

isothermal MHD shock condition with different values of τ are taken to match with inward integrations from different $x_*(3)$s at x_m, which produces α versus v locus as shown in Figure E4. The information of these isothermal MHD Shocks is displayed in Table E3, and the properties in Figure E5-E6.
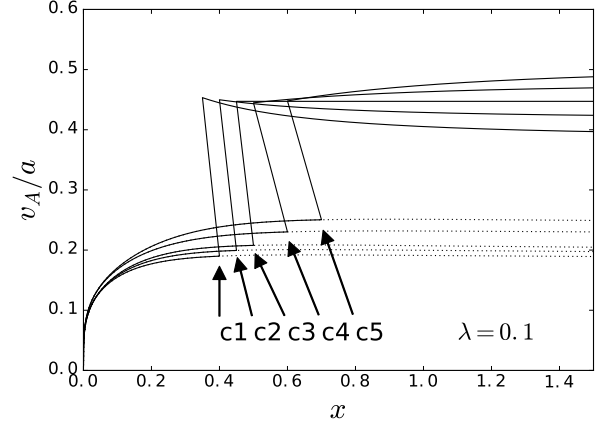
Figure E2. The v_A/a versus x diagram of Class III converging isothermal MHD Shocks relevant to Group 1 MHD free-fall collapse solutions with $\lambda = 0.1$, corresponding to Figure E1 and Table E1.
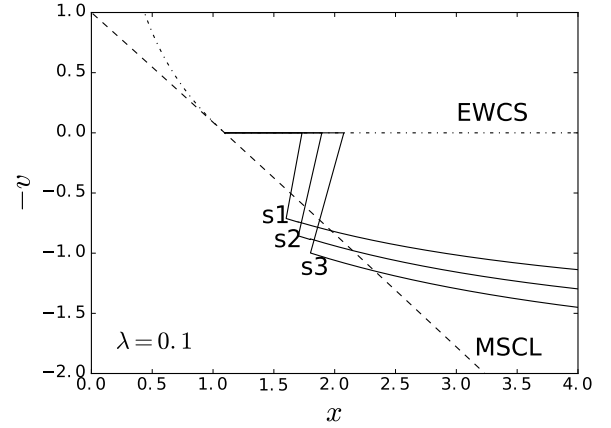

Figure E3. The $-v$ versus x diagram of Class III converging isothermal MHD Shocks relevant to the EWSC with $\lambda = 0.1$ and parameters (the curve/MHD solution label L, the meeting point x_m): (s1, 1.7), (s2, 1.8), (s3, 1.9) (see Table E2 for more information). The dashed dotted line is the non-shock EWCS. The dashed line is the MSCL.

Table E3. Three Class III converging isothermal MHD shock solutions constructed by Group 2 MHD free-fall collapse solutions with $\lambda = 0.1$, where $x_2 = 500.0$ for calculating approximately the values of V and A.

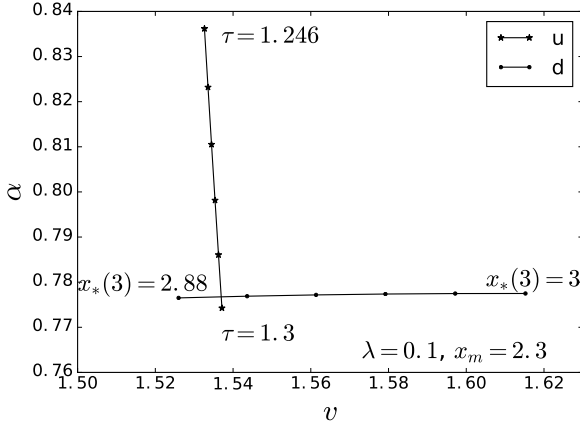| x_{sd}	x_{su}	τ	$x_*(3)$	V	A	L
1.2	1.2223	1.0186	1.5500	0.939	3.282	c6
2.2	2.8534	1.2970	2.8931	2.74	6.306	c7
3.0	4.8954	1.6318	3.7296	3.58	7.634	c8

Figure E4. Examples of the α versus v locus in search of the Class III converging isothermal MHD Shock involving the Group 2 MHD free-fall collapse solutions with $\lambda = 0.1$ and $x_m = 2.3$. The upstream locus (marked by asterisks, labelled by 'u') is formed by outward integrations starting from $x_*(2) = 1.165$ involving shocks at $x_{ud} = 2.2$ with different values of τ in the range of $1.246 \sim 1.3$. $x_*(2) = 1.165$ is where the MHD free-fall collapse solution that crosses the MSCL first at $x_*(1) = 1.2 \times 10^{-6}$ with the central accretion rate $m_0 = 2.399 \times 10^{-6}$ crosses the MSCL for the second time. The downstream locus (marked by solid dot, labelled by 'd') is produced by inward integrations as Type 1 eigensolutions with different starting points $x_*(3)$s on the MSCL in the range of $2.88 \sim 3$.
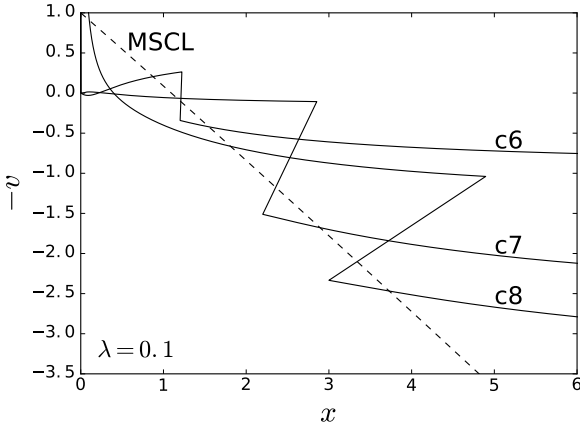

Figure E6. The v_A/a versus x diagram of Class III converging isothermal MHD Shocks relevant to Group 2 MHD free-fall collapse solutions with $\lambda = 0.1$, corresponding to Figure E5 and Table E3.

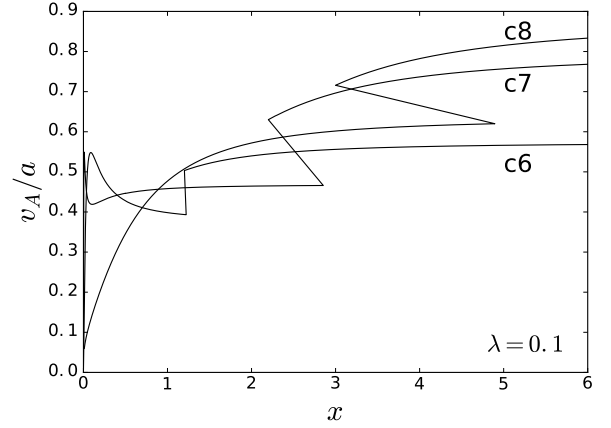This paper has been typeset from a TeX/LaTeX file prepared by the author.

Figure E5. The $-v$ versus x diagram of Class III converging isothermal MHD Shocks relevant to Group 2 MHD free-fall collapse solutions with $\lambda = 0.1$ and parameters (the curve/MHD solution label L, number of the stagnation point (i.e. at which $v = 0$) N, the point at which the MHD free-fall collapse solution crosses the MSCL for the first time $x_*(1)$, the point at which the MHD free-fall collapse solution crosses the MSCL for the second time $x_*(2)$, the meeting point x_m, the central accretion rate of the MHD free-fall collapse solution m_0): (c8, 1, 0.10306, 1.81092, 3.2, 0.1948), (c6, 2, 1.28·10^{-4}, 0.873, 1.25, 2.5513 × 10^{-4}), (c7, 3, 1.2 × 10^{-6}, 1.165, 2.3, 2.3990 × 10^{-6}). More information is contained in Table E3. The dashed line corresponds to the MSCL.